国際学会

1. Numano, T., Xu, J., Futakuchi, M., Fukamachi, K., Furukawa, F., Tsuda, H., and Suzui, M. (2013). Effect of anatase type nanosized titanium dioxide particles on the rat lung and cultured macrophage 2013AACR.
2. SUZUI, M., NUMANO, T., FUKAMACHI, K., FUTAKUCHI, M., and TSUDA, H. (2013). Lack of carcinogenic effect of multiwall carbon nanotubes on the rat lung at 2 and 52 weeks after pulmonary instillation. 2013AACR.
3. Fukamachi, K., Ohshima, Y., Futakuchi, M., Tsuda, H., and Suzui, M. (2013). A rat model of preclinical diagnosis of lung carcinoma. 72nd Annual Meeting of the Japanese Cancer Association Yokohama, Oct.3 - Oct. 5.
4. SUZUI, M., IKENAGA, S., ISODA, Y., NUMANO, T., FUKAMACHI, K., FUTAKUCHI, M., and TSUDA, H. (2013). Inflammation profile and gene expression status induced by intratracheal instillation of the multiwall carbon nanotube into rat lung. The XIII International Congress of Toxicology 2013 Seoul, Korea, June 30. - July 4.

G．知的財産権の出願・登録状況（予定を含む）

1．特許取得

無し

2．実用新案登録

無し

3．その他

特に無し。

Ⅲ．研究成果の刊行に関する一覧表

書籍

著者氏名	論文タイトル名	書籍全体の編集者名	書　籍　名	出版社名	出版地	出版年	ページ

雑誌

発表者氏名	論文タイトル名	発表誌名	巻号	ページ	出版年
Miyoshi N, Iuliano L, Tomono S, Ohshima H	Implications of cholesterol autoxidation products in the pathogenesis of inflammatory diseases.	Biochem Biophys Res Commun	446	702-708	2014
Ohba T, Sawada E, Suzuki Y, Yamamura, H, Ohya S & Imaizumi Y.	Enhancement of Ca^{2+} influx facilitated by membrane hyperpolarization due to ATP-sensitive K^{+} channel openers enhances ciliary beating in mouse airway ciliated cells.	J Pharmacol Exp Ther	347	145–153	2013
Teruya Ohba, Jiegou Xu, David Bedell Alexander, Akane Yamada, Jun Kanno, Akihiko Hirose, Hiroyuki Tsuda, Yuji Imaizumi.	MWCNT causes extensive damage to the ciliated epithelium of the trachea of rodents	J Toxicological Science	in press		2014
Sakai Y, Fukamachi K, Futakuchi M, Miyoshi I, Tsuda H, Suzui M, Hayashi H	A novel transgenic mouse model carrying human tribbles related protein 3 (TRB3) gene and its site specific phenotype	Biol Pharm Bull	in press		
Nunamo T, Xu J, Futakuchi M, Alexander DB, Furukawa F, Kanno J, Hirose A, Tsuda H, Suzui M.	Comparative study of toxic effects of anatase and rutile type nanosized titanium dioxide particles in vivo and in vitro.	Asian Pac J Cancer Prev	15	929-935	2014
Xu J, Futakuchi M, Alexander DB, Fukamachi K, Numano T, Suzui M, Shimizu H, Omori T, Kanno J, Hirose A, Tsuda H.	Nanosized zinc oxide particles do not promote DHPN-induced lung carcinogenesis but cause reversible epithelial hyperplasia of terminal bronchioles.	Arch Toxicol	88	65-75	2014
Suzui M, Morioka T, Yoshimi N.	Colon preneoplastic lesions in animal models.	Arch Toxicol	26	335-341	2013
Sakai Y, Fukamachi K, Futakuchi M, Hayashi H, Suzui M.	Promotive effects of cell proliferation and chromosomal instability induced tribbles-related protein 3 in mouse mammary tumor cells	Oncol Rep	30	64-70	2013

Fukamachi K, Tanaka H, Sakai Y, Alexander DB, Futakuchi M, Tsuda H, Suzui M.	A novel reporter rat strain that express LacZ upon Cre-mediated recombination.	Genesis	51	268-274	2013
Yabushita S, Fukamachi K, Tanaka H, Fukuda T, Sumida K, Deguchi Y, Mikata K, Nishioka K, Kawamura S, Uwagawa S, Suzui M, Alexander DB, Tsuda H.	Metabolomic and transcriptomic profiling of human K-ras oncogene transgenic rats with pancreatic ductal adenocarcinomas.	Carcinogenecis	34	1251-1259	2013
Yabushita S, Fukamachi K, Kikuchi F, Ozaki M, Miyata K, Sukata T, Deguchi Y, Tanaka H, Kakehashi A, Kawamura S, Uwagawa S, Wanibuchi H, Suzui M, Alexander DB, Tsuda H.	Twenty-one proteins up-regulated in human H-ras oncogene transgenic rat pancreas cancers are up-regulated in human pancreas cancer	Pancreas	42	1034-1039	2013
Masuda M, Toh S, Wakasaki T, Suzui M, Joe AK.	Somatic evolution of head and neck cancer-biological robustness and latent vulnerability	Mol Oncol	7	14-28	2013

Ⅳ. 研究成果の刊行物・別冊

Biochemical and Biophysical Research Communications 446 (2014) 702–708

Contents lists available at ScienceDirect

Biochemical and Biophysical Research Communications

journal homepage: www.elsevier.com/locate/ybbrc

Review

Implications of cholesterol autoxidation products in the pathogenesis of inflammatory diseases

Noriyuki Miyoshi [a,*], Luigi Iuliano [b,*], Susumu Tomono [a], Hiroshi Ohshima [a]

[a] Laboratory of Biochemistry, Graduate School of Integrated Pharmaceutical and Nutritional Sciences, Graduate Program in Food and Nutritional Sciences, University of Shizuoka, Shizuoka 422-8526, Japan

[b] Department of Medico-Surgical Sciences and Biotechnologies, Laboratory of Vascular Biology and Mass Spectrometry, Sapienza University of Rome, Latina 04100, Italy

ARTICLE INFO

Article history:
Available online 9 January 2014

Keywords:
Cholesterol autoxidation
Inflammation
Oxidative stress
Oxysterols
Secosterol

ABSTRACT

There is rising interest in non-enzymatic cholesterol oxidation because the resulting oxysterols have biological activity and can be used as non-invasive markers of oxidative stress *in vivo*. The preferential site of oxidation of cholesterol by highly reactive species is at C_7 having a relatively weak carbon–hydrogen bond. Cholesterol autoxidation is known to proceed via two distinct pathways, a free radical pathway driven by a chain reaction mechanism (type I autoxidation) and a non-free radical pathway (type II autoxidation). Oxysterols arising from type II autoxidation of cholesterol have no enzymatic correlates, and singlet oxygen ($^1\Delta gO_2$) and ozone (O_3) are the non-radical molecules involved in the mechanism. Four primary derivatives are possible in the reaction of cholesterol with singlet oxygen via ene addition and the formation of 5α-, 5β-, 6α- and 6β-hydroxycholesterol preceded by their respective hydroperoxyde intermediates. The reaction of ozone with cholesterol is very fast and gives rise to a complex array of oxysterols. The site of the initial ozone reaction is at the $\Delta_{5,6}$ –double bond and yields 1,2,3-trioxolane, a compound that rapidly decomposes into a series of unstable intermediates and end products. The downstream product 3β-hydroxy-5-oxo-5,6-secocholestan-6-al (sec-A, also called 5,6-secosterol), resulting from cleavage of the B ring, and its aldolization product (sec-B) have been proposed as a specific marker of ozone-associated tissue damage and ozone production *in vivo*. The relevance of specific ozone-modified cholesterol products is, however, hampered by the fact sec-A and sec-B can also arise from singlet oxygen via Hock cleavage of 5α-hydroperoxycholesterol or via a dioxietane intermediate. Whatever the mechanism may be, sec-A and sec-B have no enzymatic route of production *in vivo* and are reportedly bioactive, rendering them attractive biomarkers to elucidate oxidative stress-associated pathophysiological pathways and to develop pharmacological agents.

Contents

Abbreviations: Aβ, amyloid-β; Chol-OOHs, cholesterol hydroperoxides; C27 3β -HSD, 3β-hydroxy-Δ^5-C_{27}-steroid oxidoreductase; DNPH, dinitrophenyl hydrazine; DH, dansyl hydrazine; GP, Girard P; GC/MS, gas chromatography/mass spectrometry; HMP, 2-hydrazino-1-methylpyridine; LC/MS, liquid chromatography/mass spectrometry; LOD, limit of detection; LOO°, lipid peroxyl radicals; LO°, lipid alkoxyl radicals; MBP, myelin basic protein; MPO, myeloperoxidase; PBH, pyrenebutyric hydrazine; PHGPx, phospholipid-hydroperoxide glutathione peroxidase; sec-A, 3β-hydroxy-5-oxo-5,6-secocholestan-6-al; secA-COOH, 3β-hydroxy-5-oxo-secocholestan-6-oic acid; sec-B, 3β-hydroxy-5β-hydroxy-B-norcholestane-6β-carboxaldehyde; secB-COOH, 3β-hydroxy-5β-hydroxy-B-norcholestane-6-oic acid; 5α-Chol-OOH, 5α-cholesterol-hydroperoxide; 5β-Chol-OOH, 5β-cholesterol-hydroperoxide; 6α-Chol-OOH, 6α-cholesterol-hydroperoxide; 6β-Chol-OOH, 6β-cholesterol-hydroperoxide; 7α-OHC, 7α-hydroxycholesterol; 7α-Chol-OOH, 7α-cholesterol-hydroperoxide; 7β-Chol-OOH, 7β-cholesterol-hydroperoxide; 24-OHC, 24-hydroxycholesterol; 27-OHC, 27-hydroxycholesterol.

* Corresponding authors. Fax: +81 54 264 5530 (N. Miyoshi). Fax: +39 06 62 29 1089 (L. Iuliano).
E-mail addresses: miyoshin@u-shizuoka-ken.ac.jp (N. Miyoshi), luigi.iuliano@uniroma1.it (L. Iuliano).

0006-291X/$ - see front matter © 2014 Elsevier Inc. All rights reserved.
http://dx.doi.org/10.1016/j.bbrc.2013.12.107

1. Introduction

Oxysterols are derivatives of cholesterol containing one or more oxygen atoms, other than the OH group on C_3, as hydroxyl, keto, epoxide or peroxyde group – that is mounted on the A and B ring or on the side chain. Oxysterols can be generated either enzymatically, mainly by the group of cytochrome (CYP) P450 family, or by autoxidation [1]. In brief, in biological systems oxygenation on side-chain is almost exclusively enzymatic, while that on the A and B ring can occur both enzymatically and by autoxidation.

Oxysterols arising from enzymatic synthesis can be used as markers of their respective cytochrome activity. Circulating 7α-hydroxycholesterol (7α-OHC), a starting intermediate in the biosynthesis of bile acids [2], correlates with the activity of CYP7A1 [3], 7α-hydroxy-4-cholesten-3-one, a conversion product of 7α-OHC is formed by the microsomal 3β-hydroxy-Δ^5-C_{27}-steroid oxidoreductase (C27 3β-HSD) [4], 4β-hydroxycholesterol can be used as an endogenous marker of CYP3A4 and CYP3A5 activity [5], 24S-hydroxycholesterol (24-OHC) is the product of the brain-specific cholesterol 24-hydroxylase (CYP46A1) [6,7], 27-hydroxycholesterol (27-OHC) is formed by the mitochondrial enzyme sterol 27-hydroxylase (CYP27A1), which is widely distributed in tissues [8,9]. Examples of oxysterols forming enzymes different than the cyt450 family are cholesterol 25-hydroxylase [10] and oxidosqualene cyclase [11], which produce 25-hydroxycholesterol and 24(S),25-epoxycholesterol, respectively, and cholesterol epoxide hydrolase that converts 5,6-epoxydes into cholesterol-triol [12].

The susceptibility of cholesterol to non-enzymatic oxidation has generated considerable interest in oxysterols as potential markers for the non-invasive study of oxidative stress *in vivo*. Additional interest in oxysterols stems from the biological activity of many oxysterols that is useful to elucidate pathophysiological pathways in human diseases and for pharmacological purposes [13]. Cholesterol autoxidation proceeds via two distinct pathways, a free radical pathway driven by a chain reaction mechanism (type I) and a non-free radical pathway (type II), which is driven stoichiometrically by highly reactive oxygen species [13,14]. The unique cholesterol double bond between carbons 5 and 6 is the most vulnerable site for oxidation by free radicals and highly reactive species [15].

2. Cholesterol autoxidation

Type I autoxidation involves initiation and propagation reactions. Free radicals provide the initiation step by hydrogen abstraction, formation of a carbon centered radical and subsequent oxygen capture. Afterwards, the process advances through free radical intermediates – including, peroxyl radicals ($LOO^{\cdot}$) and alkoxyl radicals ($LO^{\cdot}$) – that in turn recruit additional non-oxidized molecules and provoke the spreading of the process via a chain-reaction, the propagation phase.

Despite the hydrogen bond-dissociation energy of C_7-cholesterol is higher than the hemolytic cleavage of allylic hydrogens in polyunsaturated fatty acids [16], entropic factors determine a predominant role of cholesterol oxidation in cellular membranes [17].

A multitude of oxysterols can be formed upon type I autoxidation, but analytical issues restrain the number of species usable as markers of oxidative stress in biological matrices. The species that actually perform well on GC/MS, which is the gold standard for oxysterols measurement, are: 4α- and 7β-hydoxycholesterol, 5α,6α- and 5β,6β-epoxides, and 7-ketocholesterol [13]. Recent studies from Porter and co-workers have established the product distribution of several oxysterols obtained through the free radical chain oxidation of the cholesterol precursor 7-dehydrocholesterol [18].

In type II autoxidation the main molecules that are involved in cholesterol oxidation are the non-radical species singlet oxygen and ozone. Singlet oxygen is formed by an input of energy, such as photoactivation, the Russell mechanism, based on the decomposition of lipid hydroperoxides, and by the reactions of hypochlorous acid and hydrogen peroxide. The following primary species are possible in the reaction of cholesterol with singlet oxygen via ene addition: 5α-cholesterol-hydroperoxide (5α-Chol-OOH), 5β-cholesterol-hydroperoxide (5β-Chol-OOH), 6α-cholesterol-hydroperoxide (6α-Chol-OOH), 6β-cholesterol-hydroperoxide (6β-Chol-OOH), and Chol-1,2-dioxetane. The formation of 5α-Chol-OOH is highly favored at a rate of approximately one order of magnitude higher than that of 6α-Chol-OOH and 6β-Chol-OOH [19]. Minor products of ozone-driven cholesterol oxidation are 5α,6α- and 5β,6β-epoxides, which have been found to form in ethyl acetate [20], but their participation in a physiological environment is not reported. The 7α- and 7β-Chol-OOH are formed during the reaction of singlet oxygen with cholesterol and generated indirectly by the allylic rearrangement of 5α-Chol-OOH [21], which takes place at high peroxidation levels but is negligible under limited cholesterol oxidation (<5%) [22]. Cholesterol hydroperoxides are susceptible to 1 e^- reduction that gives rise to alkoxyl- and peroxyl-radical intermediates that, in turn, can trigger chain reactions and amplify the free radical cascade of cholesterol oxidation and the oxidative damage. All cholesterol hydroperoxides are expected to be equally susceptible to 1 e^- reduction in the presence of metal catalysts. Similar rate constants have been reported for the reduction of 5α-Chol-OOH and 6α-Chol-OOH formation during incubation with an iron-based redox cycling system in a homogeneous solution in which cholesterol was the only chain-carrying species [19]. The potency of 5α-Chol-OOH and 7α-Chol-OOH as chain initiators is comparable [23]. Cholesterol hydroperoxides (Chol-OOHs) are resistant to direct 2 e^- reduction that is catalyzed by Se-dependent glutathione peroxidase [24]. This means that Chol-OOHs have a potential long half-life in cells. The only enzyme capable of catalyzing the reduction of Chol-OOHs to stable diols, is the phospholipid-hydroperoxide glutathione peroxidase (PHGPx) [25]. However, the reduction of Chol-OOH by PHGPx is 6 times slower compared to the reduction of phospholipid hydroperoxides [26], and shows different rate constants ranging from $0.8 \times 10^2\ min^{-1}$ for 5α-Chol-OOH to $\approx 6 \times 10^2\ min^{-1}$ for 6α-Chol-OOH and 6β-Chol-OOH [19]. Thus, 5α-Chol-OOH results the most abundant product of singlet oxygen reaction with cholesterol, and the least resistant to detoxification via PHGPx. The forward products arising from type-II cholesterol autoxidation are cholesterol aldehydes.

3. Cholesterol aldehydes: ozone or not ozone?

3β-Hydroxy-5-oxo-5,6-secocholestan-6-al (sec-A), the major cholesterol ozonolysis products [20], is unstable in physiological aqueous conditions, such as culture medium containing serum, and is readily converted to its aldolization product 3β-hydroxy-5β-hydroxy-B-norcholestane-6β-carboxaldehyde (sec-B) (Fig. 1) [27]. In part, sec-A and sec-B are further converted to their oxidized forms 3β-hydroxy-5-oxo-secocholestan-6-oic acid (secA-COOH) and 3β-hydroxy-5β-hydroxy-B-norcholestane-6-oic acid (secB-COOH) in culture media and probably *in vivo* [27]. Recently, ozonolysis products of the major cholesteryl fatty acid esters transported in human LDL have been reported [28]. Under a flux of ozone, cholesteryl palmitate gives rise to palmitoyl-sec-A and palmitoyl-sec-B. Instead, ozonolysis of cholesterol esterified with unsaturated fatty acids oleate and linoleate admits the initial

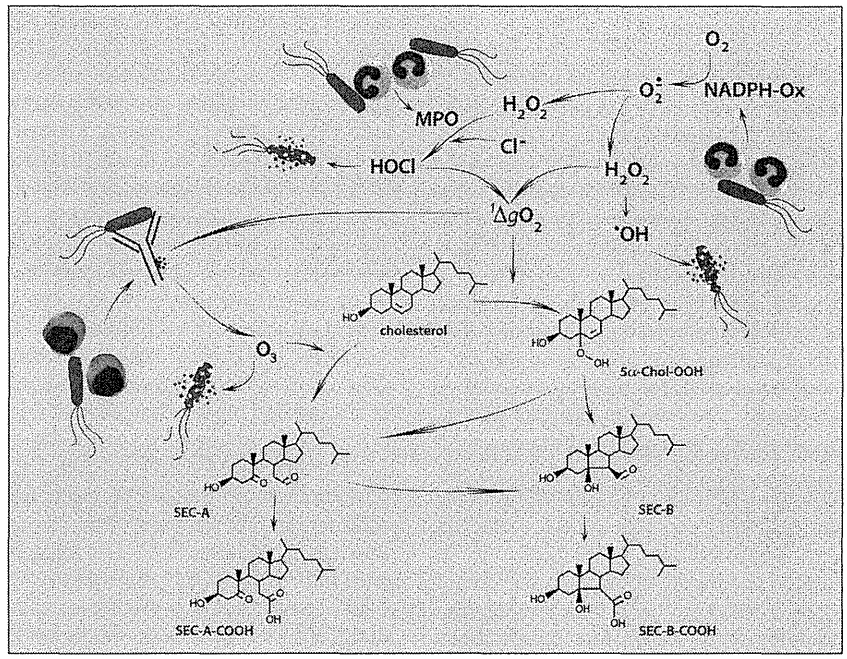

Fig. 1. Schematic representation of secosterols formation during the inflammatory response. Phagocytic cells recruited after a bacterial insult, are activated to produce highly reactive oxygen species through two enzymatic systems, i.e. NADPH-oxidase (NADPH-ox) and Myeloperoxidase (MPO) that contribute to bacterial killing. The formation of ozone by an antibody catalyzed reaction that uses singlet oxygen as substrate, has been proposed by Wentworth et al. [32,70,71] as an ancestral primary immune-response mechanism additional to the well-known superoxide-hydrogen peroxide-HOCl system. Ozone (O_3) and singlet oxygen ($^1\Delta gO_2$) may catalyze the formation of secosterols by promoting cholesterol autoxidation.

isolation of cholesteryl-9-oxononanoate and the subsequent appearance of both the fatty acid and cholesteryl moiety oxidation products, i.e. 9-oxononanoyl-sec-A and 9-oxononanoyl-sec-B [28]. These compounds derived from cholesterol/cholesterol esters ozonolysis exert potent biological activities including the denaturation of proteins and strong cytotoxicity in different cells lines (see below). High levels of sec-A and sec-B have been detected in human atherosclerotic plaques [29] and tissues samples of brains affected by neurodegeneration, such as Alzheimer's disease and Lewy body dementia [30,31], suggesting that increased formation of these compounds may be associated with inflammation-related diseases. Wentworth et al. [29] conducted pioneering works on secosterols and advised sec-A and sec-B as potential diagnostic markers of endogenous ozone production. They proposed a novel mechanisms for the unprecedented formation of ozone *in vivo* consisting of reactive oxygen species cascade (Fig. 1): (a) superoxide generation by activated neutrophil, (b) dismutation into hydrogen peroxide, (c) hypochlorous acid (HOCl) formation by myeloperoxidase (MPO), (d) singlet oxygen generation by the reaction of HOCl and hydrogen peroxide, and afterwards (e) formation of ozone from the singlet oxygen in an antibody-catalyzed water oxidation pathway [32,33]. A similar mechanism for the production of ozone-like reactive species from singlet oxygen in an amino acids-catalyzed water oxidation pathway was also reported [34]. However others have argued against the ozone-dependent mechanism of sec-A formation *in vivo* [35–37], and pointed out an alternative pathway for the formation of sec-A and sec-B. Uemi et al. [38] proposed a mechanism based on the Hock cleavage of 5α-Chol-OOH or a Chol-1,2-dioxetane intermediate formed by the reaction of cholesterol with singlet oxygen. Others provided evidence for sec-A and sec-B generation by the reaction of cholesterol with singlet oxygen produced by 1-methylnaphthalene-4-endoperoxide in phosphate buffer [39], and by the MPO–H_2O_2–Cl system [39]. Taken together these data point to a duplicate mechanism of sec-A and sec-B formation involving either ozone or singlet oxygen. Garner et al. [40] recently reported the development of a specific fluorogenic probes for ozone detections that, eventually, may help to investigate the role of ozone in pathophysiology. Being sec-B the predominant species formed during singlet oxygen-mediated cholesterol oxidation (sec-B is about 5–10 times higher than sec-A), the ratio sec-A to sec-B has been proposed as a surrogate measure to decipher the ozone-dependent and independent oxidation of cholesterol [39]. On the other hand, sec-A occurs as the dominant species formed by ozone in aqueous buffer system [41], and by phorbol-12-myristate-3-acetate-activated neutrophil in culture [27]. In addition, we were able to observe a time-dependent elevation of sec-A and sec-B in plasma after injecting lipopolysaccaride to C57BL/6j mice, but not in MPO-deficient mice. Besides, basal levels of sec-A and sec-B in the plasma of MPO-deficient mice were lower than the value found in wild type mice, but sec-A was barely detectable [27]. Sec-B was shown to be formed by aldolization of sec-A and, also, in an ozone-independent pathway via 5α-OOH-Chol or cholesterol-1,2-dioxetane [38]. Sec-B detected in the plasma of MPO-deficient mice, therefore, could be formed by the reaction of cholesterol with singlet oxygen generated *in vivo*, although its exact origin is currently unknown. Taken together these findings advise the occurrence of ozone-mediated reaction *in vivo* even if no conclusive evidences so far could be drawn for ozone production *in vivo*.

4. Biological activity of secosterols

The aldehydic function of secosterols is highly reactive and efficiently forms Schiff bases with ε- or N-terminal amino groups of proteins and with phosphatidylethanolamine, relevantly connected with atherosclerosis and a number of diseases associated with protein misfolding.

Wentworth et al. [29] reported that incubation of human LDL with either sec-A or sec-B led to time-dependent changes in the circular dichroism spectra of apoB-100, consistent with an altered

secondary structure, and increased atherogenicity, e.g. the secosterol-modified LDL was avidly taken up by macrophage leading to foam cell formation. Sec-A was shown to randomly modify the 6 different Lys residues of ApoC-II, as well as apolipoprotein that in the absence of lipids has conformational instability and undergoes fibrillization [42]. Sec-A accelerated ApoC-II polymerization with concurrent increase in thioflavin fluorescence [42], a signature of amyloidogenesis [43]. Interestingly, secA-COOH, which lacks the aldehydic functionality and is unable to form Schiff bases, was also able to accelerate ApoC-II fibril formation, albeit at a lesser extent, suggesting that non-covalent mechanisms may support secosterol-dependent ApoC-II amyloidogenesis [42]. These findings are relevant to the mechanisms of atherosclerosis because amyloid deposits are present in 50–60% of atherosclerotic lesions [44] and ApoC-II is a prominent component of these deposits [45]. Concentrations of secosterols are reportedly elevated in the cortex of patients with Lewy body dementia [31], a disease associated with intra-neuronal accumulation of α-synuclein in the form of amyloid fibrils or Lewy bodies. Sec-A, sec-B, and secoA-COOH have been shown to accelerate α-synuclein aggregation *in vitro*, and more interestingly secA-COOH was even more potent in forwarding the process [31]. Amyloidogenicity of amyloid-β (Aβ) is considered a crucial player of Alzheimer disease but an open question is the 2–3 order of magnitude disparity between the critical concentration to induce aggregation, which is in the micromolar range, and the actual concentration of Aβ at tissue level, which is in the nanomolar range [46]. Secosterols have been shown to effectively reduce below 100 nM the critical concentration of Aβ to aggregate [30,47]. Among the Aβ adducts with secosterol, Lys-16 Aβ modification formed amorphous aggregates fast and at very low concentrations of Aβ (20 nM), followed by the Lys-28 and Asp-1. Besides, the aggregates resulting from Lys-secosterols adducts were more toxic to primary rat cortical neuron [48]. Sec-A and sec-B in brain samples of patients affected by neurodegenerative disease approach concentrations of up 1 μM [30,49] that are suitable to covalently modify Aβ and increase its amyloidogenicity [30,31,47,50,51]. Sec-A and sec-B have been reported to induce structural change to myelin basic protein (MBP) relevant to the context of demyelinating diseases [52]. MBP accounts for approximately 30% of the total myelin protein, and is responsible for adhesion and stabilization of the intracellular surfaces of myelin layers. By reacting with MBP, secosterols have been shown to increase the surface exposure of the immunodominant epitope, decrease the surface exposure of the cathepsin D binding, and reduce the size and structural stability of MBP-induced aggregates. As a consequence of these alterations in the structure and function, MBP is unable to maintain the integrity of the myelin sheath and becomes vulnerable to autoimmune attack. In line to that which is observed with secosterol-initiated misfolding of Aβ and α-synuclein, sec-A and sec-B have been reported to induce misfolding of wild-type p53 [53]. The tumor suppressor protein p53 functions to maintain the integrity of the genome, and its activation in response to DNA damage promotes cell-cycle arrest in G1 phase or apoptosis. Upon incubation with secosterols, p53 undergoes polymerization that anticipates the formation of amyloid fibrillary aggregates. This misfolding renders p53 unable to bind to DNA and to induce transactivation of p21 [53]. Given that inflammation is the fuel for secosterols formation and that inflammation functions in all stages of tumor development, secosterols provide a chemical link to understand cancer carrying inactive p53.

Light-chain deposition disease is a severe, often fatal, clinical condition in which amyloid or amorphous deposits, as a consequence of antibody light chain aggregation, accumulate in the heart and/or kidney. Sec-A and sec-B have been reported to accelerate aggregation of human antibody kappa and lambda light chains *in vitro* under physiologically relevant conditions, causing an amorphous-type aggregation that is thioflavin and Congo red negative for both the kappa and lambda light chains [54]. Given the inflammatory microenvironment of secosterol production and its association with antibodies, the secosterol-induced protein misfolding is consistent with a pathophysiological role in light-chain deposition disease.

While the above reported studies show secosterols as playing deleterious roles by promoting misfolding of varied proteins, sec-B has unexpectedly been shown to inhibit the misfolding of a truncated murine mutant prion protein. Incubation of sec-B with a murine prion protein, paradoxically, induced stabilization of the native form of the prion and inhibited the generation of the disease-causing scrapie form [55]. The inhibition was specific for sec-B, where structural analogues were ineffective, offering a promising tool to develop new pharmacological active compounds to treat prion disease.

Additionally, secosterols have been reported to affect membrane and enzyme function. It was shown that secosterols bound phosphatidylethanolamine and phosphatidylserine via Schiff base formation, and also reduced biophysical parameters of membrane stability, which could be associated with various pathogenic insults [56–58]. Recently Genaro-Mattos and co-workers [59] reported that sec-B covalently bound and anchored cytochrome c to mitochondrial mimetic membranes, although its physiological role is still under investigation. Sec-A, but not sec-B, reportedly inhibited endothelial- and neuronal-type of nitric oxide synthase (NOS) activities, probably mediated by adduct formations with lysine residues on these enzymes [60]. The biochemical and biophysical properties of secosterols could be associated with their noxious activity on cells. Several studies have found that sec-A and sec-B induce cell death in various cell lines, including human B-lymphocytes (WI-L2), T-lymphocytes (Jurkat), vascular smooth muscle cells (VSMC), abdominal aorta endothelial cells (HAEC), murine tissue macrophages (J774.1), and an alveolar macrophage cell line (MH-S) [29]. Sathishkumar et al. [61] reported that sec-A exerted about 2-fold higher cytotoxicity than 5,6β-epoxy-Chol in hypothalamic neuron GT1-7 cells. Several pathways have been postulated for secosterol-triggered cell death, including the caspase-3/7-dependent pathway and the mitochondrial and death receptor pathway in cardiomyocyte H9c2 cells [62,63], the reactive oxygen species-dependent pathway in hypothalamic neuron GT1-7 cells [61,64], a mitochondrial death pathway in macrophage J774 cells, and the mitogen-activated protein kinase pathway in hepatocarcinoma HepG2 and Huh7 cells [65]. Moreover, secA-COOH and secB-COOH showed strong cytotoxic activities in human acute promyelocytic leukemia HL-60 cells [66]. Recently, it has been reported that 9-oxononanoyl-secA and 9-oxononanoyl-secB – ozonolysis products of cholesteryl-oleate and cholesteryl-linoleate present in human LDL – exert potent cytotoxicity towards HL-60 cells [28]. Their activity is stronger than other cytotoxic oxysterols, exhibiting EC50s of 10–20 μM, which were very similar against various cell lines tested.

5. *In vivo* detection

An overview of methods, biological samples investigated and levels of secosterols reported to date in the literature is shown in Table 1. For the analysis of sec-A and sec-B in biological or clinical samples, HPLC separation with UV, fluorescence, or MS detection have been widely employed. In general, lipid extracts of blood or tissue samples containing sec-A and sec-B are derivatized with hydrazine derivatives, such as dinitrophenylhydrazine (DNPH) [29,67,72]. To perform higher sensitivity detection, derivatization with dansyl hydrazine (DH, LOD = 1 fmol in [27,31,39]), 1-pyrenebutyric hydrazine (PBH; LOD = 10 fmol in [68]), Girard P (GP) hydra-

Table 1
Detections of sec-A and sec-B in biological samples.

Tissues/fluids	Species	Forms	Equipments	Concentrations	N	Ref
Lung	Rat (SD) exposed to ozone	Sec-A-DNPH	HPLC-UV	ND		72
		Sec-B-DNPH		ND		
Atherosclerotic plaque	Human	Sec-A-DNPH	HPLC-UV and LC-MS	6.8 - 61.3 pmol/mg	n=11	29
Plasma	Human (atherosclerotic patients)	Sec-B-DNPH		70 - 1690 nM	n=8	
Brain	Human (Alzheimer patients)	Sec-A-DNPH + Sec-B-DNPH	HPLC-UV and LC-MS	0.44 pmol/mg	n=4	30
	Human (Control)	Sec-A-DNPH + Sec-B-DNPH		0.35 pmol/mg	n=7	
Brain	Human (Lewy body dementia)	Sec-A-DNSL + Sec-B-DNSL	HPLC-F	0.21 uM	n=15	31
	Age-matched control	Sec-A-DNSL + Sec-B-DNSL		0.09 uM	n=18	
Brain	Rat	Sec-A-GP	LC-MS	~100 pg/mg		49
		Sec-B-GP		~300 pg/mg		
	Human	Sec-A-GP + Sec-B-GP		150 pg/mg		
Plasma	Mouse (C57BL/6)	Sec-A-DNSL	LC-MS/MS with IS (^{13}C-sec-A + ^{13}C-sec-B)	0.5 ± 0.2 nM	n=8	27
		Sec-B-DNSL		1.1 ± 0.3 nM	n=8	
	Mouse (C57BL/6 MPO-KO)	Sec-A-DNSL		0.03 ± 0.1 nM	n=7	
		Sec-B-DNSL		0.5 ± 0.4 nM	n=7	
Liver	Mouse (C57BL/6)	Sec-B-DNSL		126.0 ± 42.7 pmol/g	n=8	
	Mouse (C57BL/6 MPO-KO)	Sec-B-DNSL		62.2 ± 21.6 pmol/g	n=7	
Plasma	Human (healthy volunteers)	Sec-A-HMP	LC-MS/MS with IS (^{13}C-sec-A + ^{13}C-sec-B)	23.6 ± 16.6 nM	n=10	69
		Sec-B-HMP		27.3 ± 41.0 nM	n=10	
	Mouse (C57BL/6)	Sec-A-HMP		1.4 ± 0.7 pmol/g	n=3	
		Sec-B-HMP		4.3 ± 0.8 pmol/g	n=3	
Brain		Sec-A-HMP		10.4 ± 16.3 pmol/g	n=3	
		Sec-B-HMP		110.9 ± 10.6 pmol/g	n=3	
Liver		Sec-A-HMP		34.1 ± 21.6 pmol/g	n=3	
		Sec-B-HMP		161.5 ± 56.3 pmol/g	n=3	
Lung		Sec-A-HMP		29.1 ± 1.3 pmol/g	n=3	
		Sec-B-HMP		80.4 ± 1.4 pmol/g	n=3	

zine (LOD = 2.7 fmol in [49]), or 2-hydrazino-1-methylpyridine (HMP; LOD = 10–50 amol in [69]). Using these derivatizing reagents, sec-A and sec-B present in blood or tissues were detectable as secosterol–hydrazone derivatives by HPLC-fluorescence detector and LC–MS (Table 1). Griffiths and co-workers reported levels of sec-A and sec-B in rat brain of ~100 pg/mg (240 pmol/g) and ~300 pg/mg (720 pmol/g), respectively, determined after derivatization with GP hydrazine [49]. Sec-A and sec-B in human brain were also analyzed by HPLC-UV or LC–MS after derivatization with DNPH resulting in levels of (sec-A + sec-B) 0.44 pmol/mg in Alzheimer's patients ($n = 4$) and 0.35 pmol/mg in control subjects ($n = 7$) [30]. In addition, increased levels of secosterols (sec-A + sec-B) were observed in the cortex of brain affected by Lewy body dementia (0.213 μM, $n = 15$) compared to those of age-matched controls (0.093 μM, $n = 18$) in analysis done by HPLC-fluorescence detector and LC–MS after DH derivatization [31]. Wentworth and co-worker analyzed DNPH-derivatives of sec-A and sec-B in organic extracts of human atherosclerotic plaque by LC–MS, and found them in the ranges of 6.8–61.3 pmol/mg plaque [29]. Elevated levels of sec-B were also observed in the plasma of these patients (70–1690 nM) compared to those of controls subjects [29]. We have recently developed a highly sensitive isotope dilution method to detect sec-A and sec-B as HMP derivatives by LC–ESI–MS/MS, and using 3,4-^{13}C-sec-A and 3,4-^{13}C-sec-B as internal standards [69]. We found levels of sec-A and sec-B of 23.6 ± 16.6 nM and 27.3 ± 41.0 nM, respectively, in human plasma ($n \approx 10$). The levels of sec-A and sec-B were respectively 1.4 ± 0.7 and 4.3 ± 0.8 nM in the plasma, 10.4 ± 16.3 and 110.9 ± 10.6 pmol/g in the brain, 34.1 ± 21.6 and 161.5 ± 56.3 pmol/g in the liver and 29.1 ± 1.3, and 80.4 ± 1.4 pmol/g in the lung of C57BL/6j mice ($n = 3$). In addition, ozonolysis products of cholesteryl-oleate and cholesteryl-linoleate, 9-oxononanoyl-sec-A and 9-oxononanoyl-sec-B, were found in human LDL at levels of 16.5 ± 5.4 and 11.3 ± 3.9 pmol/mg LDL protein, respectively [28]. Notably, the values of cholesterol aldehydes in biological samples differ widely among the different laboratories. As sec-A is very unstable, at least the use of stable-isotope labeled internal standards in secosterol analysis is mandatory.

Although formation mechanisms of secosterols are not still fully unveiled, elevated levels of secosterols have been observed in various tissues collected from different inflammatory diseases. Sec-A, sec-B, and other related compounds including secA-COOH, secB-COOH, and 9-oxononanoyl secosterols exert strong biological activities compared to other oxysterols. Further studies are warranted to elucidate the mechanisms of secosterols formation *in vivo* and their pathological roles in relation to pathogenesis of several inflammatory diseases.

Acknowledgments

This work was supported in part by JSPS KAKENHI Grants (24680075 to NM, 24700838 to ST, and 24300257 to HO).

References

[1] I.A. Pikuleva, Cholesterol-metabolizing cytochromes P450: implications for cholesterol lowering, Expert Opin. Drug Metab. Toxicol. 4 (2008) 1403–1414.
[2] I. Bjorkhem, G. Eggertsen, Genes involved in initial steps of bile acid synthesis, Curr. Opin. Lipidol. 12 (2001) 97–103.
[3] I. Bjorkhem, E. Reihner, B. Angelin, S. Ewerth, J.E. Akerlund, K. Einarsson, On the possible use of the serum level of 7alpha-hydroxycholesterol as a marker for increased activity of the cholesterol 7alpha-hydroxylase in humans, J. Lipid Res. 28 (1987) 889–894.
[4] A. Lovgren-Sandblom, M. Heverin, H. Larsson, E. Lundstrom, J. Wahren, U. Diczfalusy, I. Bjorkhem, Novel LC–MS/MS method for assay of 7alpha-hydroxy-4-cholesten-3-one in human plasma. Evidence for a significant extrahepatic metabolism, J. Chromatogr. B: Anal. Technol. Biomed. Life Sci. 856 (2007) 15–19.
[5] U. Diczfalusy, J. Miura, H.K. Roh, R.A. Mirghani, J. Sayi, H. Larsson, K.G. Bodin, A. Allqvist, M. Jande, J.W. Kim, E. Aklillu, L.L. Gustafsson, L. Bertilsson, 4Beta-hydroxycholesterol is a new endogenous CYP3A marker: relationship to CYP3A5 genotype, quinine 3-hydroxylation and sex in Koreans, Swedes and Tanzanians, Pharmacogenet. Genomics 18 (2008) 201–208.
[6] D. Lutjohann, O. Breuer, G. Ahlborg, I. Nennesmo, A. Siden, U. Diczfalusy, I. Bjorkhem, Cholesterol homeostasis in human brain: evidence for an age-dependent flux of 24S-hydroxycholesterol from the brain into the circulation, Proc. Natl. Acad. Sci. U S A 93 (1996) 9799–9804.

[7] Y. Ohyama, S. Meaney, M. Heverin, L. Ekstrom, A. Brafman, M. Shafir, U. Andersson, M. Olin, G. Eggertsen, U. Diczfalusy, E. Feinstein, I. Bjorkhem, Studies on the transcriptional regulation of cholesterol 24-hydroxylase (CYP46A1): marked insensitivity toward different regulatory axes, J. Biol. Chem. 281 (2006) 3810–3820.
[8] N.B. Javitt, 25R,26-Hydroxycholesterol revisited: synthesis, metabolism, and biologic roles, J. Lipid Res. 43 (2002) 665–670.
[9] N.B. Javitt, Oxysteroids: a new class of steroids with autocrine and paracrine functions, Trends Endocrinol. Metab. 15 (2004) 393–397.
[10] E.G. Lund, T.A. Kerr, J. Sakai, W.P. Li, D.W. Russell, CDNA cloning of mouse and human cholesterol 25-hydroxylases, polytopic membrane proteins that synthesize a potent oxysterol regulator of lipid metabolism, J. Biol. Chem. 273 (1998) 34316–34327.
[11] J. Wong, C.M. Quinn, A.J. Brown, Synthesis of the oxysterol, 24(S), 25-epoxycholesterol, parallels cholesterol production and may protect against cellular accumulation of newly-synthesized cholesterol, Lipids Health Dis. 6 (2007) 10.
[12] G. Segala, Medina P. de, L. Iuliano, C. Zerbinati, M.R. Paillasse, E. Noguer, F. Dalenc, B. Payre, V.C. Jordan, M. Record, S. Silvente-Poirot, M. Poirot, 5,6-Epoxy-cholesterols contribute to the anticancer pharmacology of tamoxifen in breast cancer cells, Biochem. Pharmacol. 86 (2013) 175–189.
[13] L. Iuliano, Pathways of cholesterol oxidation via non-enzymatic mechanisms, Chem. Phys. Lipids 164 (2011) 457–468.
[14] A.W. Girotti, Lipid hydroperoxide generation, turnover, and effector action in biological systems, J. Lipid Res. 39 (1998) 1529–1542.
[15] O. Wintersteiner, S. Bergström, The products formed by the action of oxygen on colloidal solutions of cholesterol, J. Biol. Chem. 137 (1941) 785–786.
[16] H.W. Gardner, Oxygen radical chemistry of polyunsaturated fatty acids, Free Radical Biol. Med. 7 (1989) 65–86.
[17] D. Neshchadin, F. Palumbo, M.S. Sinicropi, I. Andreu, G. Gescheidta, M.A. Miranda, Topological control in radical reactions of cholesterol in model dyads, Chem. Sci. 4 (2013) 1608–1614.
[18] L. Xu, Z. Korade, N.A. Porter, Oxysterols from free radical chain oxidation of 7-dehydrocholesterol: product and mechanistic studies, J. Am. Chem. Soc. 132 (2010) 2222–2232.
[19] W. Korytowski, M. Wrona, A.W. Girotti, Radiolabeled cholesterol as a reporter for assessing one-electron turnover of lipid hydroperoxides, Anal. Biochem. 270 (1999) 123–132.
[20] J. Gumulka, L.L. Smith, Ozonization of cholesterol, J. Am. Chem. Soc. 105 (1983) 1972–1979.
[21] L.J. Athelstan, J. Beckwith, A.G. Davies, I.G.E. Davison, A. Maccoll, M.H. Mruzek, The mechanism of the rearrangement of allylic hydroperoxides 5α-hydroperoxy-3-β-hydroxycholest-6ene- and 7α-hydroperoxy-3-beta-hydroxycholest-5-ene, J. Chem. Soc., Perkin Trans. 22 (1989) 815–824.
[22] W. Korytowski, G.J. Bachowski, A.W. Girotti, Photoperoxidation of cholesterol in homogeneous solution, isolated membranes, and cells: comparison of the 5 alpha- and 6 beta-hydroperoxides as indicators of singlet oxygen intermediacy, Photochem. Photobiol. 56 (1992) 1–8.
[23] W. Korytowski, P.G. Geiger, A.W. Girotti, Lipid hydroperoxide analysis by high-performance liquid chromatography with mercury cathode electrochemical detection, Methods Enzymol. 300 (1999) 23–33.
[24] J.P. Thomas, A.W. Girotti, Photooxidation of cell membranes in the presence of hematoporphyrin derivative: reactivity of phospholipid and cholesterol hydroperoxides with glutathione peroxidase, Biochim. Biophys. Acta 962 (1988) 297–307.
[25] J.P. Thomas, M. Maiorino, F. Ursini, A.W. Girotti, Protective action of phospholipid hydroperoxide glutathione peroxidase against membrane-damaging lipid peroxidation. In situ reduction of phospholipid and cholesterol hydroperoxides, J. Biol. Chem. 265 (1990) 454–461.
[26] J.P. Thomas, P.G. Geiger, M. Maiorino, F. Ursini, A.W. Girotti, Enzymatic reduction of phospholipid and cholesterol hydroperoxides in artificial bilayers and lipoproteins, Biochim. Biophys. Acta 1045 (1990) 252–260.
[27] S. Tomono, N. Miyoshi, H. Shiokawa, T. Iwabuchi, Y. Aratani, T. Higashi, H. Nukaya, H. Ohshima, Formation of cholesterol ozonolysis products in vitro and in vivo through a myeloperoxidase-dependent pathway, J. Lipid Res. 52 (2011) 87–97.
[28] N. Miyoshi, N. Iwasaki, S. Tomono, T. Higashi, H. Ohshima, Occurrence of cytotoxic 9-oxononanoyl secosterol aldehydes in human low-density lipoprotein, Free Radical Biol. Med. 60 (2013) 73–79.
[29] P. Wentworth Jr., J. Nieva, C. Takeuchi, R. Galve, A.D. Wentworth, R.B. Dilley, G.A. DeLaria, A. Saven, B.M. Babior, K.D. Janda, A. Eschenmoser, R.A. Lerner, Evidence for ozone formation in human atherosclerotic arteries, Science 302 (2003) 1053–1056.
[30] Q. Zhang, E.T. Powers, J. Nieva, M.E. Huff, M.A. Dendle, J. Bieschke, C.G. Glabe, A. Eschenmoser, P. Wentworth Jr., R.A. Lerner, J.W. Kelly, Metabolite-initiated protein misfolding may trigger Alzheimer's disease, Proc. Natl. Acad. Sci. U S A 101 (2004) 4752–4757.
[31] D.A. Bosco, D.M. Fowler, Q. Zhang, J. Nieva, E.T. Powers, P. Wentworth Jr., R.A. Lerner, J.W. Kelly, Elevated levels of oxidized cholesterol metabolites in Lewy body disease brains accelerate alpha-synuclein fibrilization, Nat. Chem. Biol. 2 (2006) 249–253.
[32] P. Wentworth Jr., J.E. McDunn, A.D. Wentworth, C. Takeuchi, J. Nieva, T. Jones, C. Bautista, J.M. Ruedi, A. Gutierrez, K.D. Janda, B.M. Babior, A. Eschenmoser, R.A. Lerner, Evidence for antibody-catalyzed ozone formation in bacterial killing and inflammation, Science 298 (2002) 2195–2199.
[33] B.M. Babior, C. Takeuchi, J. Ruedi, A. Gutierrez, P. Wentworth Jr., Investigating antibody-catalyzed ozone generation by human neutrophils, Proc. Natl. Acad. Sci. U S A 100 (2003) 3031–3034.
[34] K. Yamashita, T. Miyoshi, T. Arai, N. Endo, H. Itoh, K. Makino, K. Mizugishi, T. Uchiyama, M. Sasada, Ozone production by amino acids contributes to killing of bacteria, Proc. Natl. Acad. Sci. U S A 105 (2008) 16912–16917.
[35] H. Sies, Ozone in arteriosclerotic plaques: searching for the "smoking gun", Angew. Chem., Int. Ed. Engl. 43 (2004) 3514–3515.
[36] L.L. Smith, Oxygen, oxysterols, ouabain, and ozone: a cautionary tale, Free Radical Biol. Med. 37 (2004) 318–324.
[37] W.A. Pryor, K.N. Houk, C.S. Foote, J.M. Fukuto, L.J. Ignarro, G.L. Squadrito, K.J. Davies, Free radical biology and medicine: it's a gas, man!, Am J. Physiol. Regul. Integr. Comp. Physiol. 291 (2006) R491–R511.
[38] M. Uemi, G.E. Ronsein, S. Miyamoto, M.H. Medeiros, Mascio P. Di, Generation of cholesterol carboxyaldehyde by the reaction of singlet molecular oxygen [O_2 ($^1\Delta_g$)] as well as ozone with cholesterol, Chem. Res. Toxicol. 22 (2009) 875–884.
[39] S. Tomono, N. Miyoshi, K. Sato, Y. Ohba, H. Ohshima, Formation of cholesterol ozonolysis products through an ozone-free mechanism mediated by the myeloperoxidase–H_2O_2–chloride system, Biochem. Biophys. Res. Commun. 383 (2009) 222–227.
[40] A.L. Garner, C.M. St Croix, B.R. Pitt, G.D. Leikauf, S. Ando, K. Koide, Specific fluorogenic probes for ozone in biological and atmospheric samples, Nat. Chem. 1 (2009) 316–321.
[41] A.D. Wentworth, B.D. Song, J. Nieva, A. Shafton, S. Tripurenani, P. Wentworth Jr., The ratio of cholesterol 5,6-secosterols formed from ozone and singlet oxygen offers insight into the oxidation of cholesterol in vivo, Chem. Commun. (Cambridge, U.K.) 21 (2009) 3098–3100.
[42] C.R. Stewart, L.M. Wilson, Q. Zhang, C.L. Pham, L.J. Waddington, M.K. Staples, D. Stapleton, J.W. Kelly, G.J. Howlett, Oxidized cholesterol metabolites found in human atherosclerotic lesions promote apolipoprotein C-II amyloid fibril formation, Biochemistry 46 (2007) 5552–5561.
[43] D.M. Hatters, C.E. MacPhee, L.J. Lawrence, W.H. Sawyer, G.J. Howlett, Human apolipoprotein C-II forms twisted amyloid ribbons and closed loops, Biochemistry 39 (2000) 8276–8283.
[44] C. Rocken, J. Tautenhahn, F. Buhling, D. Sachwitz, S. Vockler, A. Goette, T. Burger, Prevalence and pathology of amyloid in atherosclerotic arteries, Arterioscler. Thromb. Vasc. Biol. 26 (2006) 676–677.
[45] L.A. Medeiros, T. Khan, J.B. El Khoury, C.L. Pham, D.M. Hatters, G.J. Howlett, R. Lopez, K.D. O'Brien, K.J. Moore, Fibrillar amyloid protein present in atheroma activates CD36 signal transduction, J. Biol. Chem. 279 (2004) 10643–10648.
[46] P.D. Mehta, T. Pirttila, B.A. Patrick, M. Barshatzky, S.P. Mehta, Amyloid beta protein 1–40 and 1–42 levels in matched cerebrospinal fluid and plasma from patients with Alzheimer disease, Neurosci. Lett. 304 (2001) 102–106.
[47] J. Bieschke, Q. Zhang, E.T. Powers, R.A. Lerner, J.W. Kelly, Oxidative metabolites accelerate Alzheimer's amyloidogenesis by a two-step mechanism, eliminating the requirement for nucleation, Biochemistry 44 (2005) 4977–4983.
[48] K. Usui, J.D. Hulleman, J.F. Paulsson, S.J. Siegel, E.T. Powers, J.W. Kelly, Site-specific modification of Alzheimer's peptides by cholesterol oxidation products enhances aggregation energetics and neurotoxicity, Proc. Natl. Acad. Sci. U S A 106 (2009) 18563–18568.
[49] K. Karu, M. Hornshaw, G. Woffendin, K. Bodin, M. Hamberg, G. Alvelius, J. Sjovall, J. Turton, Y. Wang, W.J. Griffiths, Liquid chromatography-mass spectrometry utilizing multi-stage fragmentation for the identification of oxysterols, J. Lipid Res. 48 (2007) 976–987.
[50] H. Komatsu, L. Liu, I.V. Murray, P.H. Axelsen, A mechanistic link between oxidative stress and membrane mediated amyloidogenesis revealed by infrared spectroscopy, Biochim. Biophys. Acta 1768 (2007) 1913–1922.
[51] I.V. Murray, L. Liu, H. Komatsu, K. Uryu, G. Xiao, J.A. Lawson, P.H. Axelsen, Membrane-mediated amyloidogenesis and the promotion of oxidative lipid damage by amyloid beta proteins, J. Biol. Chem. 282 (2007) 9335–9345.
[52] N.K. Cygan, J.C. Scheinost, T.D. Butters, P. Wentworth Jr., Adduction of cholesterol 5,6-secosterol aldehyde to membrane-bound myelin basic protein exposes an immunodominant epitope, Biochemistry 50 (2011) 2092–2100.
[53] J. Nieva, B.D. Song, J.K. Rogel, D. Kujawara, L. Altobel 3rd, A. Izharrudin, G.E. Boldt, R.K. Grover, A.D. Wentworth, P. Wentworth Jr., Cholesterol secosterol aldehydes induce amyloidogenesis and dysfunction of wild-type tumor protein p53, Chem. Biol. 18 (2011) 920–927.
[54] J. Nieva, A. Shafton, L.J. Altobell 3rd, S. Tripuraneni, J.K. Rogel, A.D. Wentworth, R.A. Lerner, P. Wentworth Jr., Lipid-derived aldehydes accelerate light chain amyloid and amorphous aggregation, Biochemistry 47 (2008) 7695–7705.
[55] J.C. Scheinost, D.P. Witter, G.E. Boldt, J. Offer, P. Wentworth Jr., Cholesterol secosterol adduction inhibits the misfolding of a mutant prion protein fragment that induces neurodegeneration, Angew. Chem., Int. Ed. Engl. 48 (2009) 9469–9472.
[56] E. Wachtel, D. Bach, R.F. Epand, A. Tishbee, R.M. Epand, A product of ozonolysis of cholesterol alters the biophysical properties of phosphatidylethanolamine membranes, Biochemistry 45 (2006) 1345–1351.
[57] D. Bach, E. Wachtel, I.R. Miller, Kinetics of Schiff base formation between the cholesterol ozonolysis product 3-beta-hydroxy-5-oxo-5,6-secocholestan-6-al and phosphatidylethanolamine, Chem. Phys. Lipids 157 (2009) 51–55.
[58] D. Bach, R.F. Epand, R.M. Epand, I.R. Miller, E. Wachtel, The oxysterol 3beta-hydroxy-5-oxo-5,6-secocholestan-6-al changes the phase behavior and

structure of phosphatidylethanolamine–phosphatidylcholine mixtures, Chem. Phys. Lipids 164 (2011) 672–679.

[59] T.C. Genaro-Mattos, P.P. Appolinario, K.C. Mugnol, C. Bloch Jr., I.L. Nantes, Mascio.P. Di, S. Miyamoto, Covalent binding and anchoring of cytochrome c to mitochondrial mimetic membranes promoted by cholesterol carboxyaldehyde, Chem. Res. Toxicol. 26 (2013) 1536–1544.

[60] Y.L. Lai, S. Tomono, N. Miyoshi, H. Ohshima, Inhibition of endothelial- and neuronal-type, but not inducible-type, nitric oxide synthase by the oxidized cholesterol metabolite secosterol aldehyde: implications for vascular and neurodegenerative diseases, J. Clin. Biochem. Nutr. 50 (2012) 84–89.

[61] K. Sathishkumar, S.N. Murthy, R.M. Uppu, Cytotoxic effects of oxysterols produced during ozonolysis of cholesterol in murine GT1-7 hypothalamic neurons, Free Radical Res. 41 (2007) 82–88.

[62] K. Sathishkumar, M. Haque, T.E. Perumal, J. Francis, R.M. Uppu, A major ozonation product of cholesterol, 3β-hydroxy-5-oxo-5,6-secocholestan-6-al, induces apoptosis in H9c2 cardiomyoblasts, FEBS Lett. 579 (2005) 6444–6450.

[63] K. Sathishkumar, X. Gao, A.C. Raghavamenon, N. Parinandi, W.A. Pryor, R.M. Uppu, Cholesterol secoaldehyde induces apoptosis in H9c2 cardiomyoblasts through reactive oxygen species involving mitochondrial and death receptor pathways, Free Radical Biol. Med. 47 (2009) 548–558.

[64] K. Sathishkumar, X. Xi, R. Martin, R.M. Uppu, Cholesterol secoaldehyde, an ozonation product of cholesterol, induces amyloid aggregation and apoptosis in murine GT1-7 hypothalamic neurons, J. Alzheimers Dis. 11 (2007) 261–274.

[65] S. Anticoli, M. Arciello, A. Mancinetti, Martinis.M. De, L. Ginaldi, L. Iuliano, C. Balsano, 7-Ketocholesterol and 5,6-secosterol modulate differently the stress-activated mitogen-activated protein kinases (MAPKs) in liver cells, J. Cell Physiol. 222 (2010) 586–595.

[66] S. Tomono, Y. Yasue, N. Miyoshi, H. Ohshima, Cytotoxic effects of secosterols and their derivatives on several cultured cells, Biosci. Biotechnol. Biochem. 77 (2013) 651–653.

[67] K. Wang, E. Bermudez, W.A. Pryor, The ozonation of cholesterol: separation and identification of 2,4-dinitrophenylhydrazine derivatization products of 3 beta-hydroxy-5-oxo-5,6-secocholestan-6-al, Steroids 58 (1993) 225–229.

[68] F.V. Mansano, R.M. Kazaoka, G.E. Ronsein, F.M. Prado, T.C. Genaro-Mattos, M. Uemi, Mascio.P. Di, S. Miyamoto, Highly sensitive fluorescent method for the detection of cholesterol aldehydes formed by ozone and singlet molecular oxygen, Anal. Chem. 82 (2010) 6775–6781.

[69] S. Tomono, N. Miyoshi, M. Ito, T. Higashi, H. Ohshima, A highly sensitive LC–ESI–MS/MS method for the quantification of cholesterol ozonolysis products secosterol-A and secosterol-B after derivatization with 2-hydrazino-1-methylpyridine, J. Chromatogr., B: Anal. Technol. Biomed. Life Sci. 879 (2011) 2802–2808.

[70] D. Datta, N. Vaidehi, X. Xu, W.A. Goddard 3rd, Mechanism for antibody catalysis of the oxidation of water by singlet dioxygen, Proc. Natl. Acad. Sci. U S A 99 (2002) 2636–2641.

[71] A.D. Wentworth, L.H. Jones, P. Wentworth Jr., K.D. Janda, R.A. Lerner, Antibodies have the intrinsic capacity to destroy antigens, Proc. Natl. Acad. Sci. U S A 97 (2000) 10930–10935.

[72] W.A. Pryor, K. Wang, E. Bermudez, Cholesterol ozonation products as biomarkers for ozone exposure in rats, Biochem. Biophys. Res. Commun. 188 (1992) 618–623.

1521-0103/347/1/145–153$25.00
THE JOURNAL OF PHARMACOLOGY AND EXPERIMENTAL THERAPEUTICS

http://dx.doi.org/10.1124/jpet.113.205138
J Pharmacol Exp Ther 347:145–153, October 2013

Enhancement of Ca^{2+} Influx and Ciliary Beating by Membrane Hyperpolarization due to ATP-Sensitive K^+ Channel Opening in Mouse Airway Epithelial Cells

Teruya Ohba, Eiji Sawada, Yoshiaki Suzuki, Hisao Yamamura, Susumu Ohya, Hiroyuki Tsuda, and Yuji Imaizumi

Department of Molecular and Cellular Pharmacology, Graduate School of Pharmaceutical Sciences (T.O., E.S., Y.S., H.Y., Y.I.) and Nanomaterial Toxicology Project (H.T.), Nagoya City University, Nagoya, Japan; and Department of Pharmacology, Division of Pathological Sciences, Kyoto Pharmaceutical University, Kyoto, Japan (S.O.)

Received March 25, 2013; accepted August 5, 2013

ABSTRACT

Among the several types of cells composing the airway epithelium, the ciliary cells are responsible for one of the most important defense mechanisms of the airway epithelium: the transport of inhaled particles back up into the throat by coordinated ciliary movement. Changes in the cytoplasmic Ca^{2+} concentration ($[Ca^{2+}]_i$) are the main driving force controlling the ciliary activity. In mouse ciliary cells, membrane hyperpolarization from −20 to −60 mV under whole-cell voltage-clamp induced a slow but significant $[Ca^{2+}]_i$ rise in a reversible manner. This rise was completely inhibited by the removal of Ca^{2+} from the extracellular solution. Application of diazoxide, an ATP-dependent K^+ channel opener, dose-dependently induced a membrane hyperpolarization (EC_{50} = 2.3 μM), which was prevented by the addition of 5 μM glibenclamide. An inwardly rectifying current was elicited by the application of 10 μM diazoxide and suppressed by subsequent addition of 5 μM glibenclamide. Moreover, the application of 10 μM diazoxide induced a significant $[Ca^{2+}]_i$ rise and facilitated ciliary movement. Multi-cell reverse-transcription polymerase chain reaction analyses and immunocytochemical staining suggested that the subunit combination of Kir6.2/SUR2B and possibly also Kir6.1/SUR2B is expressed in ciliary cells. The confocal Ca^{2+} imaging analyses suggested that the $[Ca^{2+}]_i$ rise induced by diazoxide occurred preferentially in the apical submembrane region. In conclusion, the application of a K_{ATP} channel opener to airway ciliary cells induces membrane hyperpolarization and thereby induces a $[Ca^{2+}]_i$ rise via the facilitation of Ca^{2+} influx through the non–voltage-dependent Ca^{2+} permeable channels. Therefore, a K_{ATP} opener may be beneficial in facilitating ciliary movement.

Introduction

The regulation of K^+ channel conductance is suggested to be a critical issue in the therapy of asthma and/or chronic obstructive pulmonary disease (Pelaia et al., 2002; Malerba et al., 2010). The activation of the ATP-sensitive K^+ (K_{ATP}) channel, the large conductance Ca^{2+}-activated K^+ (BK) channel, or the intermediate conductance Ca^{2+}-activated K^+ (IK) channel by specific modulators induces the following: bronchodilation, reduced airway hyperresponsiveness, reduced mucus production and cough, suppressed airway inflammation, and the remodeling of the preclinical models of asthma and chronic obstructive pulmonary disease (Malerba et al., 2010).

Ciliary cells play a fundamental role in the airway self-defense system by removing foreign materials from the airways in functional combinations with the other types of epithelial cells. The motile cilia in the airway epithelium are the engines for mucociliary clearance, which is a mechanism responsible for cleaning the airways of inhaled particles. The ciliary beating observed in the human airway epithelium is principally due to a slow constitutive rate of beating caused by inherent and spontaneous dynein ATPase activity. The cilia can increase their beating frequency by the activation of several different control mechanisms, one of these being changes in the intracellular Ca^{2+} concentration ($[Ca^{2+}]_i$) (Evans and Sanderson, 1999; Schmid and Salathe, 2011). Aside from the regulatory effects of calcium on the ciliary beating rate, calcium is also involved in the complex task of synchronizing the beat among the cilia of one single cell as well as between the cilia on multiple cells (Schmid and Salathe, 2011).

This investigation was supported by a Grant-in-Aid for Scientific Research on Priority Areas [Grant 23136512] (to Y.I.) from the Ministry of Education, Culture, Sports, Science, and Technology in Japan; and by a Grant-in-Aid for Scientific Research [Grant 23390020] (to Y.I.) from the Japan Society for the Promotion of Science. This work was also supported by Health and Labor Sciences Research grants from the Ministry of Health, Labor and Welfare, Japan [Research on Risk of Chemical Substance 21340601, H19-kagaku-ippan-006, and H22-kagaku-ippan-005] (to H.T.).
T.O. and E.S. contributed equally to this study.
dx.doi.org/10.1124/jpet.113.205138

ABBREVIATIONS: BK, large conductance Ca^{2+}-activated K^+ channel; $[Ca^{2+}]_i$, intracellular Ca^{2+} concentration; CBF, ciliary beating frequency; DPBS, Dulbecco's phosphate-buffered saline; fluo-4/AM, fluo-4 acetoxymethyl ester; fura-2/AM, fura-2 acetoxymethyl ester; K_{ATP} channel, ATP-sensitive K^+ channel; NGS, normal goat serum; PBS, phosphate-buffered saline; PCR, polymerase chain reaction; SUR, sulfonylurea receptor; VDCC, voltage-dependent Ca^{2+} channel.

Initially, K_{ATP} channels were identified as the key molecules for insulin secretion in pancreatic β-cells; they are now well known to be ubiquitously expressed in a variety of tissues as the molecular combination of channel-forming Kir6.x subunits and sulfonylurea receptors (SURs) (Clark and Proks, 2010; Flagg et al., 2010; Hibino et al., 2010). Although the expression of K_{ATP} channels has been reported in alveolar cells (Trinh et al., 2007) and cell lines derived from human airway epithelial tissues (Trinh et al., 2008), their functional expression in ciliary cells has not yet been documented. Previous studies have revealed that ATP and acetylcholine are major endogenous stimulants that facilitate ciliary beating by activating the purinoceptors and by increasing $[Ca^{2+}]_i$, which, in turn, may induce membrane hyperpolarization via the activation of Ca^{2+}-dependent K^+ channels (Weiss et al., 1992; Tarasiuk et al., 1995). However, conflicting reports have been published on whether changes in the membrane potential can significantly affect the ciliary beat frequency (Ma et al., 2002). Therefore, the present study was undertaken to elucidate the effects of K_{ATP} openers on ciliary beating rates and to determine the underlying mechanisms of the changes. The effects of K_{ATP} openers on ciliary beating may be a key issue in evaluating their therapeutic potentials for respiratory diseases.

Materials and Methods

Animals. C57BL/6N male mice (Japan SLC, Hamamatsu, Japan), 8 to 12 weeks old, were used. All experiments were carried out in accordance with the Guiding Principles for the Care and Use of Laboratory Animals of the Japanese Pharmacological Society and also with the approval of the Ethics Committee of Nagoya City University.

Isolation of Single Ciliary Cells. The tracheas were removed from the mice. The epithelium was separated from the cartilage and cut into squares of approximately 1 × 1 mm. The tissue was maintained in Dulbecco's phosphate-buffered saline (DPBS) containing (in mM): 137 NaCl, 2.7 KCl, 0.9 $CaCl_2$, 0.5 $MgCl_2$, 8 Na_2HPO_4, 1.47 KH_2PO_4, and 5 glucose, pH 7.4. The epithelium was incubated for 25 minutes at 37°C in DPBS supplemented with 13 U/ml papain (Sigma-Aldrich, St. Louis, MO), 1 mg/ml bovine serum albumin (Sigma-Aldrich), and 1 mg/ml 1,4-dithiothreitol (Wako Pure Chemicals, Osaka, Japan). After incubation, the solution was replaced with DPBS. The cells were then dispersed several times with a fire-polished Pasteur pipette. The isolated cells were immediately used following the cell dispersion. All of the experiments were carried out at room temperature (25°C).

Multicell Reverse-Transcription Polymerase Chain Reaction. Approximately 40 ciliary cells were collected by the glass electrode of ~2-30 μm in diameter. Total RNA was extracted from them using NucleoSpin RNA XS (Macherey Nagel, Düren, Germany) and reverse-transcribed using oligo$(dT)_{12\text{-}18}$ primer and SuperScript II reverse transcriptase (Invitrogen, Carlsbad, CA). The solution without RTase was used as a negative control. The polymerase chain reaction (PCR) amplification profile using KOD-Plus-Neo (TOYOBO, Tokyo, Japan) and GeneAmp PCR System 2700 (Applied Biosystems, Foster City, CA) was as follows: a 10-second denaturation step at 98°C, a 30-second annealing step at 55°C, and a 60-second primer extension step at 72°C for 35 cycles. Gene products were analyzed by 2.0% agarose gel electrophoresis.

PCR Primers. The following PCR primers were used: for mouse Kir6.1/Kcnj8 (GenBank Accession No. NM_008428), (+) 5′-CAA GTG ACC ATT GGG TTT GGA-3′ and (−) 5′-CGT TGA TGA TCA GAC CCA CGA-3′ (100 bp); Kir6.2/Kcnj11 (NM_010602), (+) 5′-CAA GAA AGG CAA CTG CAA CGT-3′ and (−) 5′-TGT GTG GCC ATT TGA GGT CCA-3′ (101 bp); SUR1/Abcc8 (NM_011510), (+) 5′-AGT GAA GCC CCC TGA GGA CCT-3′ and (−) 5′-GAT GAA GGC ATT CAT CCA CCA-3′ (103 bp); SUR2/Abcc9 (NM_021041 and NM_011511), (+) 5′-TAC GAA CAT CAT CGA CCA GCA-3′ and (−) 5′-AAA CAC GGG TGT AGC ATA GGA-3′ (109 bp); β-actin/Actb (NM_007393), 5′-AGG CCA ACC GTG AAA AGA TG-3′ and (−) 5′-ACC AGA GGC ATA CAG GGA CA-3′ (101 bp). The specific primers for the spliced variant analysis of SUR2 were designed as follows: for mouse SUR2A/Abcc9A (NM_021041), (+) 5′-TCT TCT ATT GTG GAT GCA GGC CT-3′ and (−) 5′-CTA CTT GTT GGT CAT CAC CAA AGT-3′ (129 bp); SUR2B/Abcc9B (NM_011511), (+) 5′-CAC ACC ATT CTG ACT GCA GAC CT-3′ and (−) 5′-TCA CAT GTC TGC ACG GAC AAA CGA-3′ (129 bp).

Immunocytochemistry. Polyclonal antimouse Kir6.2 (APC-020) and control antigen were purchased from Alomone Laboratories (Jerusalem, Israel). Polyclonal antibodies to Kir6.1 (R-14), SUR1 (H-80), SUR2A (M-19), SUR2B (C-15) and each blocking peptide were purchased from Santa Cruz Biotechnology, Inc. (Dallas, TX). Dissociated ciliary cells were settled down on coverslips precoated with poly-L-lysine (Matsunami Glass Industry, Osaka, Japan). These cells were fixed with 4% paraformaldehyde for 20 minutes and permeabilized with 0.2% Triton/phosphate-buffered saline (PBS) for 15 minutes at room temperature. After rinsing in PBS containing 1% normal goat serum (NGS), the cells were preincubated for 1 hour with 10% NGS/PBS to minimize nonspecific binding of antibodie, and incubated successively with 1:100 diluted antibodies for 12 hours. Primary antibodies were extensively washed with 1% NGS/PBS and incubated with Alexa 488-conjugated antirabbit IgG goat or Alexa 488-conjugated antigoat IgG rabbit antiserum (Molecular Probe, Eugene, OR) for 1 hour. Immunostained cells were observed using an A1R laser-scanning confocal fluorescent microscope (Nikon, Tokyo, Japan) equipped with a fluorescent microscope (ECLIPSE Ti; Nikon), an objective lens (Plan Apo 60× 1.40 NA oil immersion; Nikon), and NIS Elements software (version 3.10; Nikon). The excitation wavelength from the multiargon laser (Melles Griot, Carlsbad, CA) for Alexa 488 was 488 nm, and the emission light was collected by a band-pass filter (525/50 nm).

Electrophysiological Recordings. A whole-cell patch clamp was applied to a single ciliary cell with a patch pipette using a CEZ-2400 amplifier (Nihon Kohden, Tokyo, Japan) as previously described (Imaizumi et al., 1989; Yamamura et al., 2012). The membrane currents and voltage signals were stored and analyzed using a Digidata 1440A and a pCLAMP 10.2 (Axon Instruments, Foster City, CA). The ciliary cells were clamped at a holding potential of −40 mV, and a descending ramp protocol from +40 to −120 mV for 500 milliseconds was performed every 10 seconds. In some experiments, membrane potentials from single ciliary cells were measured under the current-clamp mode in whole-cell configuration.

Measurement of the Ca^{2+} Fluorescence Ratio and the Ca^{2+} Images. The airway ciliary cells were loaded with 10 μM fura-2 acetoxymethyl ester (fura-2/AM; Molecular Probes) in a standard HEPES solution for 45 minutes at room temperature. The fura-2 fluorescent signals were measured using the Argus/HiSCA imaging system (Hamamatsu Photonics, Hamamatsu, Japan). In some experiments, in which simultaneous measurements of $[Ca^{2+}]_i$ and membrane potential were taken, ciliary cells were loaded with 100 μM fluo-4 (Molecular Probes) by diffusion from the recording pipette (Funabashi et al., 2010). The Ca^{2+} images were scanned every 2 seconds.

Intracellular Ca^{2+} Images by Use of Fluo-4/AM and Confocal Fluorescent Microscopy. The airway ciliary cells were loaded with 10 μM fluo-4 acetoxymethyl ester (fluo-4/AM; Molecular Probes) in a standard HEPES solution for 45 minutes at room temperature. The cytosolic Ca^{2+} images were obtained using the aforementioned laser-scanning confocal fluorescent microscope and NIS Elements software. The excitation wavelength for fluo-4 was 488 nm, and the emission wavelength was collected by a bandpass filter (525/50 nm). The resolution of the microscope was 0.414 μm per pixel and 2.02 μm to the *Z*-axis direction. The confocal images were scanned over a full frame (512 × 512 pixels) every 2 seconds.

Membrane Potential Measurements by Voltage-Sensitive Fluorescent Dye. The membrane potential was measured as previously reported (Yamazaki et al., 2011) using 100 nM $DiBAC_4(3)$ (Dojin,

Kumamoto, Japan), a bis-barbituric acid oxonol dye with an excitation maximum at approximately 488 nm. The data were collected and analyzed using the Argus/HiSCA imaging system. The sampling interval of the $DiBAC_4(3)$ fluorescence measurements was every 5 seconds.

Measurement of Ciliary Beating Frequency. The ciliary beating frequency (CBF) of the tracheal airway ciliary cell (Shiima-Kinoshita et al., 2004; Kawakami et al., 2004) was measured at 100 Hz using a high-speed resolution CCD camera (C9100-12, Hamamatsu Photonics). Prior to the experiments, the CBFs were measured every 1 minute for 2 minutes, and the average value of these three CBFs were used as the basal CBF (CBF_0) in the HEPES-buffered solution. Any changes in the CBF were expressed as a CBF ratio.

Solutions. An extracellular solution was made using a standard HEPES-buffered solution composed of the following (in mM): 137 NaCl, 5.9 KCl, 2.2 $CaCl_2$, 1.2 $MgCl_2$, 14 glucose, and 10 HEPES. The pH of the solution was adjusted with NaOH to 7.4. The K_{ATP} current was measured in a 40 mM K^+ HEPES-buffered solution composed of the following (in mM): 99.7 NaCl, 40 KCl, 2.2 $CaCl_2$, 1.2 $MgCl_2$, 14 glucose, and 10 HEPES. The pH of the solution was adjusted with NaOH to 7.4. The pipette solution for electrical recordings contained the following (in mM): 140 KCl, 4 $MgCl_2$, 2 ATP-Na_2, 0.05 EGTA, 10 HEPES. The pH of the solution was adjusted with KOH to 7.2. All experiments were undertaken at room temperature to avoid fura-2 trapping in organelles and dye leakage at 37°C.

Statistical Analysis. The pooled data are expressed as means ± S.E., and the statistical significance was examined using Student's t test for two groups and Tukey's for three or more groups. P values < 0.05 were considered statistically significant. The data of the relationship between diazoxide and fluorescent signal were fitted using the following equation after normalization: $F/F_0 = 1 - (1 - C)/(1 + (K_d/[\text{diazoxide}])^n)$, where C is the component resistant, K_d is the apparent dissociation constant, [diazoxide] is the concentration, and n is the Hill coefficient (Fig. 2D).

Drugs. The pharmacological reagents were obtained from Sigma-Aldrich. Diazoxide, glibenclamide, and pinacidil were dissolved in dimethylsulfoxide at concentrations of 5 to 10 mM as a stock solution.

Results

The Effects of K_{ATP} Opener on Ciliary Beating. The ciliary movement in freshly isolated mice ciliary cells was recorded at 100 Hz using a high time-resolution video camera and analyzed using a slow image reproduction (Fig. 1A). The application of 10 μM diazoxide, a K_{ATP} channel opener, significantly increased the frequency of the ciliary movement (Fig. 1B), and the effect lasted for over 10 minutes (not shown). The addition of 5 μM glibenclamide, a K_{ATP} channel blocker, removed the diazoxide-induced enhancement of the frequency (Fig. 1B). The summarized data (Fig. 1C) indicate a significant enhancement of the frequency when 10 μM diazoxide was applied ($n = 6$, $P < 0.05$ versus control) and a significant inhibition of the frequency when 5 μM glibenclamide was added ($n = 6$, $P < 0.01$ versus diazoxide alone). Although the amplitude of the movement may also be increased by the diazoxide, those quantitative analyses could not be done during this study due to the limited time resolution of the video system.

The K_{ATP} Opener–Induced Membrane Hyperpolarization and the Subsequent Rise in $[Ca^{2+}]_i$. The membrane potential changes induced by the addition of 10 μM diazoxide in the isolated ciliary cells were measured using the voltage sensitive fluorescent dye $DiBAC_4(3)$.

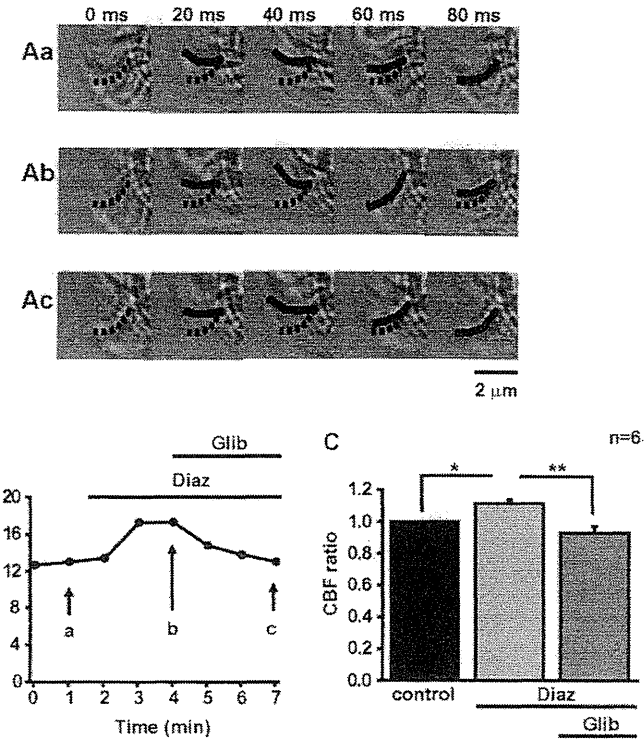

Fig. 1. The enhancement of the ciliary movement by diazoxide. (A) The ciliary movement in an epithelial cell isolated from a mouse trachea was recorded with a high-speed digital camera at 100 Hz. The CBF was directly measured from the images as shown by the dotted and solid lines. The series of images (a, b, and c) were obtained at the time shown in B. (B) The time course of CBF in HEPES-buffered solution, in the presence of 10 μM diazoxide (Diaz), and following the addition of 5 μM glibenclamide (Glib). (C) The summarized data concerning the effects of diazoxide and glibenclamide ($n = 6$). *,**$P < 0.05$ and 0.01, respectively.

The sustained decrease in the fluorescence intensity observed following the addition of 10 μM diazoxide is indicative of membrane hyperpolarization ($n = 5$, $P < 0.01$). The diazoxide-induced decrease in fluorescence intensity was completely removed by the addition of 5 μM glibenclamide ($n = 5$, $P < 0.01$; Fig. 2, A and B). The diazoxide-induced decrease in fluorescence intensity was concentration-dependent in the range of 1 and 30 μM (Fig. 2, C and D). The EC_{50} value for membrane potential of the cells treated with diazoxide was 2.3 μM, and the Hill coefficient was 3.4 ($n = 11$).

The membrane potential was also measured under current-clamp mode in freshly isolated single ciliary cells using pipette filling solution containing 140 mM KCl (see *Materials and Methods*). In all four experiments, stable recordings for over 10 minutes were successfully obtained throughout the procedure of adding two drugs sequentially; the addition of 10 μM diazoxide induced sustained membrane hyperpolarization of 3.6 ± 1.4 mV from the resting membrane potential of −18.6 ± 1.4 mV ($n = 4$). Further addition of 5 μM glibenclamide resulted in depolarization by 2.4 ± 0.5 mV ($n = 4$). Taking the initial resting membrane potential in each cell as 1.0, the potentials after the addition of diazoxide and glibenclamide were 1.20 ± 0.03 ($P < 0.01$ versus 1.0) and 1.07 ± 0.03 ($P < 0.05$ versus diazoxide alone).

The effects of the diazoxide on $[Ca^{2+}]_i$ were examined in isolated ciliary cells using fura-2/AM (Fig. 3). The application of 10 μM diazoxide increased the fluorescence ratio (F340/F380), indicating the increase in $[Ca^{2+}]_i$ ($n = 8$, $P < 0.01$). This

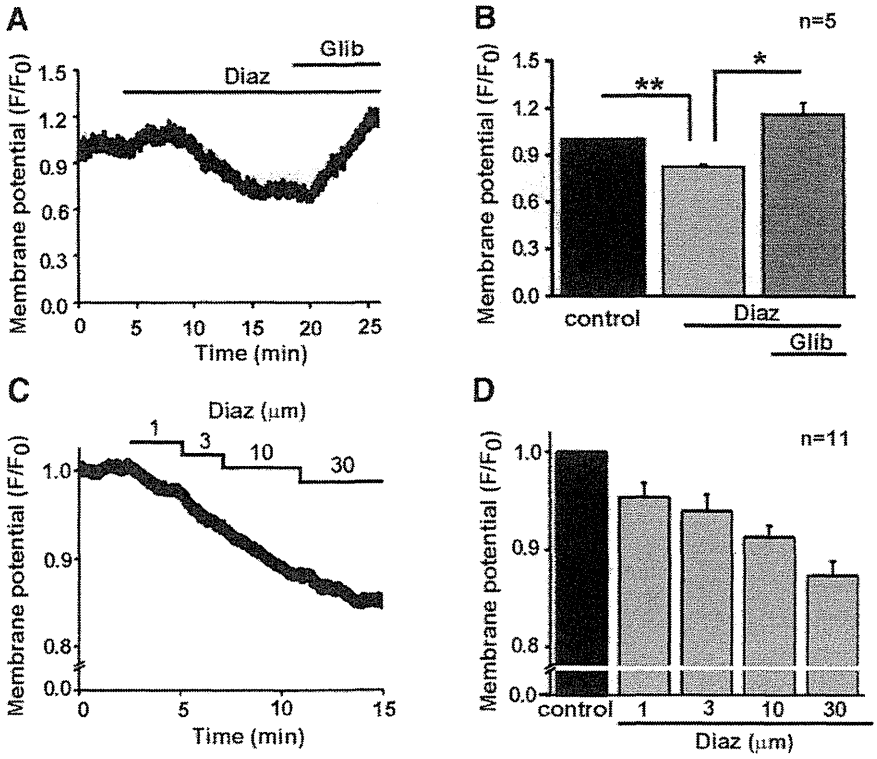

Fig. 2. The diazoxide-induced hyperpolarization of the membrane. (A) The changes in the membrane potential were monitored by the voltage-sensitive dye $DiBAC_4(3)$. The changes in the fluorescent intensity ratio (F/F_0) that were induced by the addition of 10 μM diazoxide (Diaz) and 5 μM glibenclamide (Glib) were plotted against time. The average fluorescent intensity (F) measured immediately prior to the application of the diazoxide was taken as F_0. (B) The summarized data concerning F/F_0 are shown (n = 5). *,**$P < 0.05$ and 0.01, respectively. (C) The changes in F/F_0 that were induced by the cumulative additions of diazoxide in a dose range from 1 to 30 μM were plotted against time. (D) The summarized data concerning F/F_0 are shown (n = 11). The EC_{50} value and Hill coefficient were 2.3 and 3.4 μM, respectively.

observed increase was removed by the addition of 5 μM glibenclamide (n = 8, $P < 0.01$). The $[Ca^{2+}]_i$ was also increased by the application of 10 μM pinacidil, another K_{ATP} channel opener (n = 5, $P < 0.01$), and the effect was again reversed by the addition of 5 μM glibenclamide (n = 5, $P <$ 0.01).

The Expression of ATP-Sensitive K^+ Channels in Ciliary Cells. The molecular characteristics of the K_{ATP} channels in the ciliary cells were examined by multicell reverse-transcription PCR analysis. These analyses reveal that the transcripts of Kir6.2 and SUR2B were predominantly expressed in the ciliary cells (n = 3; Fig. 4A).

To clarify protein expression of these channels, immunocytochemical analyses were performed (n = 3; Fig. 4B). Kir6.1, Kir6.2 and SUR2B proteins were detected on plasma membrane of ciliary cells. However, SUR2A did not show significant membrane surface expression. These results are consistent with those from reverse-transcription PCR analyses and strongly suggest that Kir6.2/SUR2B and possibly also Kir6.1/SUR2B are predominantly expressed in mouse ciliary cells. We did not expect to find that SUR1 showed specific expression on cilia.

The Measurement of ATP-Sensitive K^+ Channel Currents in Ciliary Cells. The K_{ATP} channel current was measured in a single ciliary cell using a whole-cell patch-clamp recording. To amplify the conductance of the Kir channel, the recordings were performed in an external solution containing 40 mM K^+. The current–voltage relationship in the control showed slight inward rectification at potentials negative to −60 mV. The inwardly rectifying current was markedly enhanced by the application of 10 μM diazoxide (Fig. 5A). The enhanced current was reduced by the addition of 5 μM glibenclamide. The reversal potential of the current component reduced by glibenclamide in the presence of diazoxide was −33 mV, which is close to the equilibrium potential of K^+ under the conditions (E_K = −32 mV). The summarized data (Fig. 5B) clearly indicate that the inward K^+ current density at −110 mV was significantly enhanced by the application of diazoxide (n = 7, $P < 0.05$ versus control) and markedly reduced by the addition of glibenclamide (n = 5; $P < 0.05$ versus diazoxide alone).

The Relationship between the Membrane Potential and $[Ca^{2+}]_i$ in the Isolated Ciliary Cells. The relationship between the membrane potential and $[Ca^{2+}]_i$ was determined in isolated ciliary cells under a whole-cell voltage-clamp. The single ciliary cells were loaded with fluo-4 from recording pipettes. A membrane hyperpolarization from −20 to −60 mV induced a slow increase in $[Ca^{2+}]_i$ (n = 4, $P < 0.01$) and the return of the potential to −20 mV removed the increase in $[Ca^{2+}]_i$ completely but at a much slower rate (n = 4, $P < 0.05$; Fig. 6, A and B). The $[Ca^{2+}]_i$ increase induced by hyperpolarization was also abolished by the withdrawal of 2.2 mM Ca^{2+} in the external solution (n = 3, $P < 0.01$; Fig. 6, C and D). As shown in Fig. 6, the time courses of $[Ca^{2+}]_i$ elevation varied widely from cell to cell, presumably due to the diversity of cell activities after isolation and also the difference in the load of Ca^{2+} indicator among cells. The summarized data indicate that the $[Ca^{2+}]_i$ increase induced by hyperpolarization from −20 to −60 mV was significant, reversible, and susceptible to external Ca^{2+}.

The Image Analyses of Local $[Ca^{2+}]_i$ Changes by Diazoxide in the Ciliary Cells. The image analyses of changes in the local $[Ca^{2+}]_i$ were performed using fluo-4/AM and a confocal fluorescent microscope. The changes in the fluorescent intensity of the three areas in the ciliated cell (central, apical, and basolateral areas indicated by "a," "b," and "c," respectively, in Fig. 7A) by the application of 10 μM

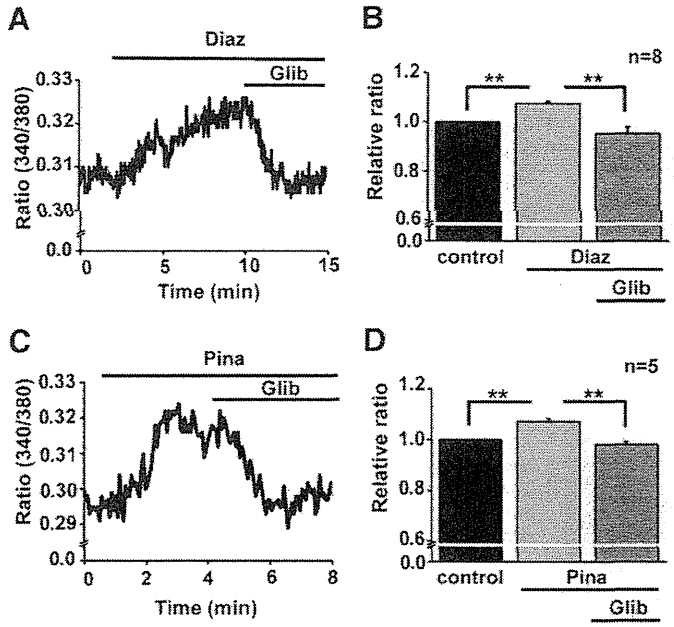

Fig. 3. The effects of diazoxide and glibenclamide on $[Ca^{2+}]_i$ in ciliated cells. (A) $[Ca^{2+}]_i$ was measured as fluorescent intensity ratio (*340/380*) in a ciliated cell that was loaded with fura-2/AM. The changes in the ratio induced by the addition of 10 μM diazoxide (Diaz) and 5 μM glibenclamide (Glib) were plotted against time. (B) The summarized data concerning the changes in F/F_0 are shown (n = 8). The averaged ratio immediately prior to the application of diazoxide was taken as 1.0. $^{**}P < 0.01$. (C) The changes in the ratio induced by the addition of 10 μM pinacidil (Pina) and 5 μM glibenclamide (Glib) were plotted against time. (D) The summarized data concerning the changes in F/F_0 are shown (n = 5). The averaged ratio immediately prior to the application of the pinacidil was taken as 1.0. $^{**}P < 0.01$.

diazoxide over time were illustrated in Fig. 7B. When the intensity at resting conditions in the cell center was taken as unity, the intensities at the apical area and the basolateral area were 1.01 ± 0.01 and 1.00 ± 0.02, respectively ($n = 9, P > 0.05$ among the three areas). After the application of 10 μM diazoxide, the intensities in each area gradually increased (Fig. 7, A and B). The rise in intensity at the apical area was more focal, faster, and larger than the rise in intensity at either the cell center or the basolateral area (Fig. 7C). The summarized data (Fig. 7D) indicate that the rise in intensity at the cell center was significantly less than the rise in intensity at the apical area ($n = 9, P < 0.05$). The rise in intensity at the basolateral area tended to be smaller than the rise in intensity at the apical area, but the difference was not significant.

In addition to the focal rise in submembrane area of the apical side (Fig. 7C, ii and iii), Ca^{2+} rise in the cytosol compartments located deep inside the cell was occasionally observed (Fig. 7C, iii, iv, and v). This type of Ca^{2+} rise was characteristic of a slow rise, deep-inside location, and nonfocal or diffused images. This specific rise was observed to varying degrees in seven of nine cells, whereas the focal and rapid Ca^{2+} rises in the apical submembrane areas were clearly detected in all nine cells examined.

Discussion

Ca^{2+} as One of the Major Factors Modulating Mucociliary Motility. In the ciliary mechanism, the basic mechanism that is responsible for the slow and constitutive rate of beating is considered to be the inherent and spontaneous dynein ATPase activity that depends mainly upon the cellular MgATP concentration (Salathe and Bookman, 1999; Ma et al., 2002). In addition, adapting to the heavier duty of particle transportation with mucus in the epithelium, the upregulation of the ciliary motility by three separate second messengers have been clarified: Ca^{2+}, c-AMP, and c-GMP (Salathe, 2007). The cross-talk among signal pathways by these three second messengers has been also revealed. Among these second messengers, Ca^{2+} has fundamental roles in facilitating CBF (Schmid and Salathe, 2011). The application of a K_{ATP} opener increases the CBF by only 10–15% above the baseline in airway ciliated cells. It has been demonstrated, however, that a 16% increase in CBF results in 56% increase in the mucociliary transport velocity in an isolated trachea (Seybold et al., 1990). In this study, the maximum response to the externally applied physiologic stimulants ATP or acetylcholine often resulted in larger rises in $[Ca^{2+}]_i$ than those induced by K_{ATP} openers. These slightly larger increases in CBF (15–30%) suggest that mucociliary clearance may therefore be substantially enhanced by K_{ATP} channel openers.

New Insight into $[Ca^{2+}]_i$ Regulation by the Membrane Potential Changes in Airway Ciliated Cells. Information concerning the influence of changes in the membrane potential on the ciliary axoneme movement is not well accumulated and still somewhat controversial. It has been reported that the application of ATP induces a $[Ca^{2+}]_i$ rise, leading to membrane hyperpolarization and facilitates the ciliary motility in frog palate and esophagus ciliated cells (Tarasiuk et al., 1995). In contrast, it has been reported that the membrane potential changes under the whole-cell voltage clamp mode does not induce a significant change in the single-airway ciliated cells of the rabbit (Ma et al., 2002). The findings in the present study clearly demonstrated that the membrane hyperpolarization achieved under a voltage clamp or induced by K_{ATP} channel openers elicited $[Ca^{2+}]_i$ rise and resulted in enhanced ciliary axoneme motility in the airway ciliated cells of the mice. The reason for the discrepancy between the studies in rabbit airway ciliated cells (Ma et al., 2002) and our results in mice is not completely clear. The changes in $[Ca^{2+}]_i$ by membrane hyperpolarization under whole-cell voltage-clamp were not recorded in the former study, presumably because the $[Ca^{2+}]_i$ was fixed by Ca^{2+}-EGTA buffer from the pipette filling solution (Ma et al., 2002). In the present study, the pipette solution contained only 50 μM EGTA and no $CaCl_2$, and the $[Ca^{2+}]_i$ rise by hyperpolarization was consistent and reversible. It is a rather common observation that prolonged membrane hyperpolarization induces a slow but sustained $[Ca^{2+}]_i$ rise in nonexcitable cells, such as T cells, chondrocytes (Funabashi et al., 2010), and vascular endothelial cells (Yamazaki et al., 2011) where the Ca^{2+} permeable channels are functionally expressed but the voltage-gated Ca^{2+} channels are not.

This study differs from the previous, conflicting study (Ma et al., 2002) based on the ATP concentrations used for experimentation. The previous study was conducted using 5 mM MgATP + 0.5 mM K_2ATP, whereas the current study was conducted using 4 mM $MgCl_2$ + 2 mM Na_2ATP. Although the basic CBF of inherent and spontaneous beating is considered to be dependent on MgATPase activity, the actual MgATP and ATP concentrations in the airway ciliated cells are unknown. It may be possible that experimental conditions in the present study influenced the CBF increase that were

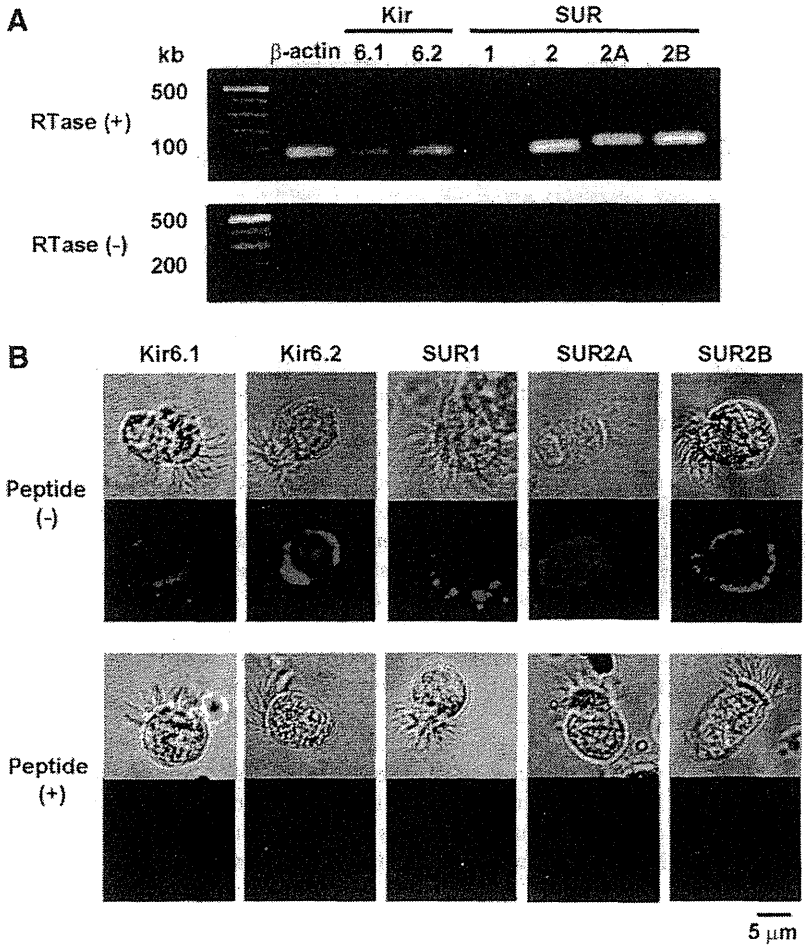

Fig. 4. The expression of K_{ATP} channel mRNA and protein in the ciliated cells. (A) The expression of Kir6.x and SURx in the ciliated cells was examined by multi-cell reverse-transcription PCR. Approximately 40 of the isolated ciliated cells in which ciliary movement was detected were collected by small pipettes in microscopic fields. Reaction solution from which RTase was omitted was used as a negative control. The expression of the transcripts for Kir6.1, Kir6.2 and SUR2 was detected. Further analyses suggest that the major transcript of SUR2 was SUR2B. (B) The protein expression was detected using immunocytochemical staining. Similarly to the results from RT-PCR, Kir6.1, Kir6.2, and SUR2B but not SUR2A were expressed on cell surface. SUR1 exhibited specific expression on cilia. The lower sets of panels indicate that the specific staining was prevented by a corresponding inhibitory peptide.

attributed to $[Ca^{2+}]_i$ rise by membrane hyperpolarization induced under voltage-clamp or by application of a K_{ATP} channel opener.

Previous studies have confirmed that the rise of $[Ca^{2+}]_i$ results in CBF enhancement, even if the underlying mechanisms are not fully understood (Schmid and Salathe, 2011). The activation of calmodulin may be involved, as this messenger protein associates with the radial spokes and the central apparatus of the flagella (Dymek and Smith, 2007) and directly interacts with dynein arms (Sakato et al., 2007). These mechanisms have been suggested for correlating the $[Ca^{2+}]_i$ rise with facilitated axoneme motility in invertebrates. In addition, it has been assumed that the $[Ca^{2+}]_i$ rise facilitates cilia motility via crosstalk with the cAMP or the cGMP mediated pathways (Braiman and Priel, 2008).

Ca^{2+} Source and Local Ca^{2+} Functions in the Regulation of Cilia Motility. In airway ciliated cells, it has been well established that two major endogenous stimulants, ATP and acetylcholine, activate P_2Y_2 and M_3 receptors, respectively. The stimuli activates phospholipase Cβ to form inositol 1,4,5 trisphosphate, which induces $[Ca^{2+}]_i$ release from the endoplasmic reticulum. In addition, sustained Ca^{2+} influx has been found to occur after Ca^{2+} release. Although the molecular mechanism of the Ca^{2+} influx is not well understood, the store-operated or receptor-operated Ca^{2+} entry may be contributing as it does in many other non-excitable cells. By some stimuli, such as stretch, the transient receptor potential vanilloid subfamily 4 (TRPV4) channel is activated to facilitate Ca^{2+} influx (Lorenzo et al., 2008).

In the present study, membrane hyperpolarization by voltage-clamp or the application of a K_{ATP} channel opener has been clearly shown to facilitate the influx of Ca^{2+}. Because airway epithelial cells are polarized structures with cilia on their apical membranes, Ca^{2+} concentrations are sufficiently high in the submembranous areas to affect ciliary beat (Braiman and Priel, 2008). It has been suggested that storage and release of Ca^{2+} in different cell compartments give rise to this apical versus basolateral concentration difference in the cytosol (Braiman et al., 2000; Braiman and Priel, 2001). In contrast, the measurement of the local $[Ca^{2+}]_i$ in this study did not show a significant Ca^{2+} gradient in the cytosol under the normal conditions (not shown). During membrane hyperpolarization by K_{ATP} openers, the Ca^{2+} rise in the apical submembrane area was significantly higher than that in the center area but not in the basolateral area.

In addition to a Ca^{2+} rise in the apical region, diazoxide occasionally induced a slower Ca^{2+} rise in the cytosolic compartments located deep inside the cells. Diazoxide reportedly interacts with the mitochondrial K_{ATP} channels as well as with plasma membrane K_{ATP} channels (Garlid et al., 1996; O'Rourke, 2004). Diazoxide reduces the mitochondrial membrane potential (or induces the mitochondrial depolarization) and thereby accelerates the release of Ca^{2+} from mitochondria (Grimmsmann and Rustenbeck, 1998; Holmuhamedov

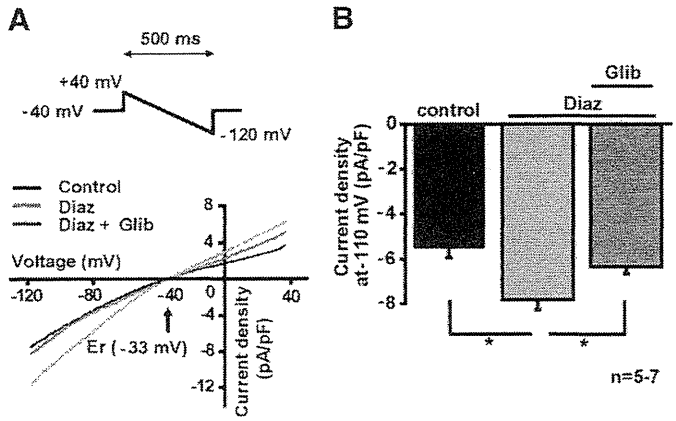

Fig. 5. K_{ATP} current in ciliated cells. (A) The membrane currents were measured from a single ciliary cell under a voltage-clamp. A ramp pulse from +40 to −120 mV (as indicated in inset) was applied in the absence (control) and the presence of 10 μM diazoxide (Diaz) and following the addition of 5 μM glibenclamide (Glib). The I-V relationships were obtained by the ramp pulse protocol. The I-V relationships in the presence of diazoxide with the absence and presence of glibenclamide crossed at −33 mV. (B) The data concerning the current density at −110 mV were summarized. The numbers of experiments were seven in the control, seven in the presence of diazoxide, and five in the co-presence of glibenclamide. $^*P < 0.05$.

et al., 1999). In addition to the Ca^{2+} influx mediated by the membrane hyperpolarization, the release of Ca^{2+} from organelles, including mitochondria, may be involved in the diazoxide-induced Ca^{2+} increase. However, it remains to be determined whether the Ca^{2+} rise induced by diazoxide deep inside the cell compartments contributes to the enhancement of the ciliary movement. Further experiments are therefore required to elucidate the mechanism underlying the local Ca^{2+} mobilization triggered by exposure to diazoxide.

K_{ATP} Channels in Ciliated Cells as a Possible Therapeutic Target. K^+ channels play a major role in maintaining the electrochemical gradient necessary for transepithelial Na^+ and Cl^- transport in secretory airway epithelia (O'Grady and Lee, 2003). The K_{ATP} channel is believed to be a significant contributor to lung physiology and pathophysiology because of the beneficial actions of openers in the lung (Fukuse et al., 2002). The molecular components of the K_{ATP} channel in the airway alveolar epithelial type II cells of the rat have been identified as the combination of Kir6.1 and SUR2B (Leroy et al., 2004). A K_{ATP} channel opener induces the relaxation of airway smooth muscle via membrane hyperpolarization and the subsequent suppression of voltage-dependent Ca^{2+} channel (VDCC) activity (Rodrigo and Standen, 2005). This relaxation is considered to be effective for the therapy of occlusive diseases, such as asthma and chronic obstructive pulmonary disease (Pelaia et al., 2002).

In this study, two K_{ATP} channel openers, diazoxide and pinacidil, and the K_{ATP} channel blocker glibenclamide were used as pharmacological tools to determine the subunits responsible for K_{ATP} channel activation in mouse ciliated cells. The combination of K_{ATP} channel subunits modulates sensitivity to K_{ATP} channel openers. Diazoxide activates SUR1 and SUR2B but not SUR2A (Yamada and Kurachi, 2005). On the other hand, pinacidil activates SUR2A and SUR2B but not SUR1. Because K_{ATP} channels in ciliated cells were activated by both diazoxide and pinacidil at <10 μM, functional K_{ATP} channels in these cells are supposed to be Kir6.x/SUR2B (Hibino et al., 2010). These results were supported by the outcomes from reverse-transcription PCR analyses and immunocytochemical staining, which showed the expression of Kir6.1, Kir6.2, and SUR2B on plasma membrane. It is interesting that immunostaining using anti-SUR1 revealed that SUR1 subunits were specifically located on cilia, but neither Kir6.1 nor Kir6.2 was detected there. SUR1 may possibly couple with other ion channels, such as the transient receptor potential channel (Woo et al., 2013). Unfortunately, the strategy of molecular manipulation by use of siRNA did not fit to this study because rat cilia disappear during cell culture for 2 days (Chang et al., 1985); the results were

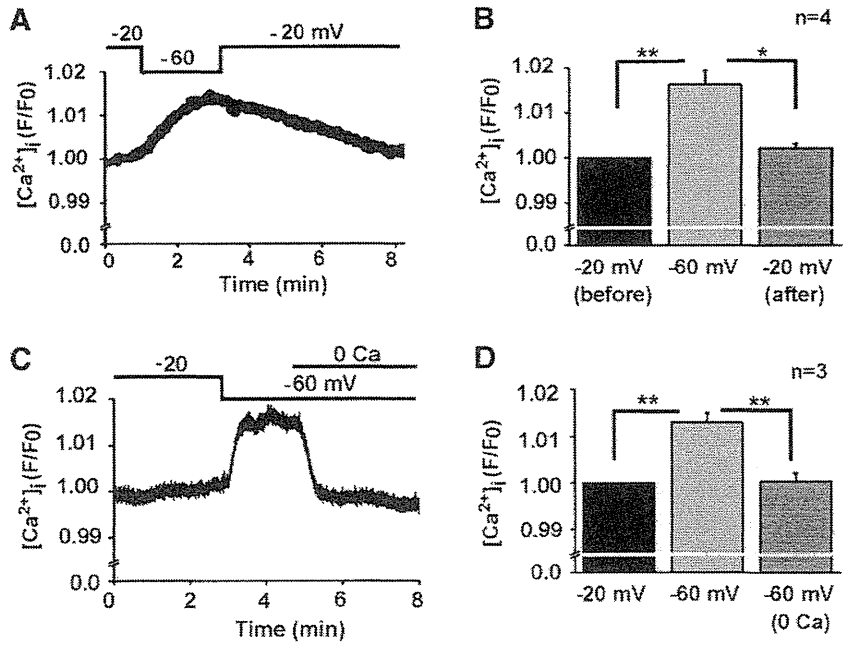

Fig. 6. $[Ca^{2+}]_i$ changes induced by the membrane hyperpolarization in ciliary the cells under a voltage-clamp. (A) The changes in $[Ca^{2+}]_i$ were monitored with the F/F_0 of the fluo4 that was applied from the recording pipette. The time course of F/F_0 during the membrane potential changes from −20 mV to −60 mV and back to −20 mV was plotted against time. The top trace indicates the clamp potential changes. (B) The summarized data concerning F/F_0 at −20 mV, at −60 mV, and back to −20 mV are shown ($n = 4$). $^*,^{**}P <$ 0.05 and 0.01, respectively. (C) The effect of Ca^{2+} removal from an external solution on the elevated F/F_0 by the hyperpolarization of the membrane was examined in a ciliary cell under a voltage clamp. The external solution was exchanged from the standard solution (2.2 mM Ca^{2+}) to a Ca^{2+} free solution (0 mM Ca^{2+}) at a potential of −60 mV as indicated in the top trace. (D) The summarized data concerning F/F_0 at −20 mV at −60 mV and following the exposure to a Ca^{2+} free solution are shown ($n = 4$). $^*,^{**}P < 0.05$ and 0.01, respectively.

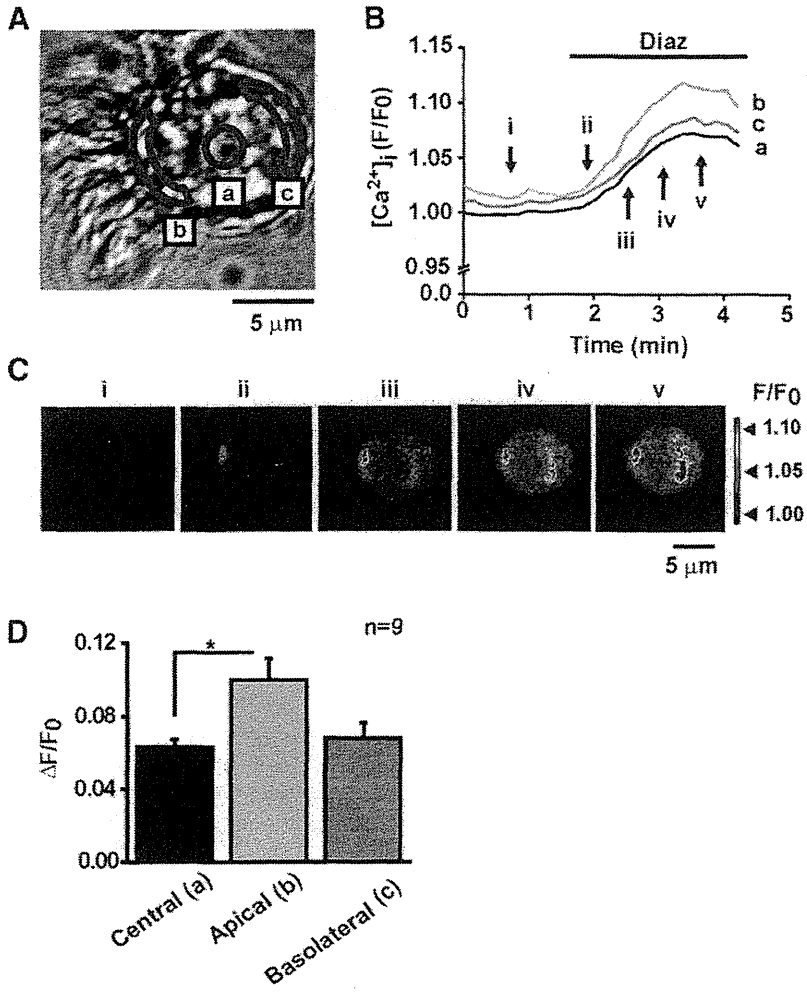

Fig. 7. The image analyses of local Ca^{2+} transients induced by diazoxide in the ciliary cells. (A) The local Ca^{2+} transients were measured by confocal fluorescent microscopy. The F/F_0 signals of fluo-4 were measured in the three areas indicated in the transfer image of the ciliary cell: "a" (center of the cell). "b" (apical submembrane area), and "c" (basolateral submembrane area). (B) Changes in F/F_0 in the three areas were plotted against time. The F_0 in area "a" was taken as 1.0 and F/F_0 in the other areas was normalized by the F_0. (C) The confocal images of $[Ca^{2+}]_i$ were obtained from the ciliary cell in the absence (i) and presence (ii, iii, and iv) of diazoxide at the timing shown in B. (D) The summarized data concerning $\Delta F/F_0$ were obtained as the differences of F/F_0 in the absence and presence of diazoxide in B (n = 9). *$P < 0.05$.

confirmed using mouse cilia in this study. Therefore, it remains to be determined whether Kir6.1 or Kir6.2 is the functionally predominant subunit in ciliated cells, whereas Kir6.2 protein expression on the plasma membrane appeared to be higher than Kir6.1.

Membrane potential recording with $DiBAC_4(3)$ allows us to get more number of results than the direct recordings under whole-cell patch clamp configuration. However, the use of $DiBAC_4(3)$ has at least three limitations. First, the artifacts by $DiBAC_4(3)$ act as a potent activator of BK channel (Morimoto et al., 2007). BK channel current component sensitive to paxilline was not recorded in ciliary cells. Second, $DiBAC_4(3)$ cannot detect fast membrane potential changes. Third, the most serious limitation is that the exact membrane potential cannot be measured by $DiBAC_4(3)$, even though calibration under voltage-clamp is available (Yamada et al., 2001). The membrane hyperpolarization induced by 10 μM diazoxide appeared to be approximately 11 mV based on the calibration. This value was apparently larger than that directly recorded under current-clamp mode (4 mV). The reason for the dissociation between two measurements is not clear. It is, however, likely that the Cl^- conductance appears to be high compared with that of K^+ in ciliated cells. When the pipette filling solution contained 140 mM Cl^-, the resting membrane potential was extremely shallow (−19 mV) and close to equilibrium potential of Cl^- rather than K^+. Under these experimental conditions, the membrane hyperpolarization attributed to the K^+ conductance increase may be smaller than what occurs under normal Cl^- gradient across the cell membrane. The intracellular Cl^- concentration varied widely depending on cell types in a range of 5 and 30 mM but is unfortunately unknown in tracheal ciliated cells. Further study is required to understand the real membrane hyperpolarization by K_{ATP} channel opening in ciliary cells.

In this study, the membrane hyperpolarization increased the influx of Ca^{2+} presumably by an unknown pathway rather than by VDCC. The membrane hyperpolarization may simply increase the transmembrane driving force for Ca^{2+} through Ca^{2+} permeable channels with non–voltage-dependent gating mechanisms. Taken together, it can be suggested that K_{ATP} channel openers may have additional benefits, including an expectorant effect, for the therapy of occlusive respiratory disorders.

In conclusion, a K_{ATP} channel composed of Kir6.2/SUR2B and possibly also Kir6.1/SUR2B is functionally expressed in ciliated cells in mice airway epithelium. The activation of a K_{ATP} channel induces membrane hyperpolarization and results in an increase in Ca^{2+}-influx through a novel, non-VDCC pathway. The enhancement of the ciliary movement by K_{ATP} openers is mainly attributable to the Ca^{2+} rise and is considered to have an additional and beneficial effect on the